Die approbierte Originalversion dieser Diplom-/Masterarbeit ist an der Hauptbibliothek der Technischen Universität Wien aufgestellt (http://www.ub.tuwien.ac.at).

The approved original version of this diploma or master thesis is available at the main library of the Vienna University of Technology (http://www.ub.tuwien.ac.at/englweb/).

MASTER THESIS

Optimization and Fabrication of Optofluidic Micro-Systems

Submitted at the Faculty of Electrical Engineering, Vienna University of Technology
in partial fulfillment of the requirements for the degree of
Master of Sciences (Diplomingenieur)

under supervision of

Univ.Prof. Dipl.-Ing. Dr.techn. Michiel J. Vellekoop
Univ.Ass. Dipl.-Ing. Michael Rosenauer

by

Emanuel Weber
Matr.Nr. 0426444
Obere Bahnzeile 5, 7361 Lutzmannsburg

November 2009

Abstract

In this project two different devices were developed. Both are placed in the field of L^2-waveguides. These are waveguides with core and cladding provided in liquid form.
The first device is a waveguide shifter. Different hydrodynamical manipulations of liquids are used to steer a liquid stream in a micro-channel. This liquid stream is used as the core of an L^2-waveguide at the same time as well. Applying different inlet velocities at different liquid inlets, results in certain distinct outlet positions for the light.
The second device is a fluorescence sensor. It takes use out of the evanescent field arising from an L^2-waveguide to excite fluorescence in a sample medium. This sample medium is brought in tight contact to the core of the waveguide. By applying different inlet velocities different analyzing situations can be generated.
This work covers the full development cycle of these two devices beginning from simulations of the design ideas, fabrication of the devices and characterization of these.
The functionality of both devices was proven in experimental setups. Both of them showed excellent working behavior.

Kurzfassung

Im Rahmen dieses Projektes wurden zwei unterschiedliche Chips entwickelt. Beide gehören in das Gebiet von Flüssigkeitslichtwellenleitern. Bei solchen Wellenleitern sind Kern und Mantel in flüssiger Form realisiert.
Der erste Chip ist ein rekonfigurierbarer Wellenleiter. Verschiedene hydrodynamische Manipulationen von Flüssigkeiten werden hierbei verwendet um einen Flüssigkeitsstrahl in einem Mikro-Kanal zu bewegen. Dieser Flüssigkeitsstrahl wird zur selben Zeit auch als Kern eines Flüssigkeitslichtwellenleiters verwendet. Durch Anlegen von unterschiedlichen Einlassgeschwindigkeiten an verschiedenen Flüssigkeitseinlässen können mehrere unterschiedliche Auslasspositionen des Lichtes erhalten werden.
Der zweite Chip ist ein Fluoreszenzsensor. Hierbei wird das evaneszente Feld eines Flüssigkeitslichtwellenleiters benutzt um Fluoreszenz in einem Testmedium zu stimulieren. Dieses Testmedium ist eng an den Kern des Wellenleiters gebracht. Durch Anlegen von unterschiedlichen Einlassgeschwindigkeiten können unterschiedliche Analysesituationen erhalten werden.
Die vorliegende Arbeit behandelt den vollständigen Entwicklungszyklus dieser beiden Chips beginnend von der Simulation der Designideen, Fertigung der Chips und Charakterisierung dieser Chips.
Die Funktion von beiden Chips wurde anhand von Experimentellen Aufbauten demonstriert. Beide zeigten exzellentes Arbeitsverhalten.

Acknowledgments

Two names should be stated here explicitly. At first, I would like to thank to Univ.Prof. Dipl.-Ing. Dr.techn. Michiel J. Vellekoop, the head of the Institute of Sensor and Actuator Systems, who provided me the possibility of writing my thesis under his supervision. Secondly, but not less important, thanks to Univ.Ass. Dipl.-Ing. Michael Rosenauer who supported me in any technical manner.
Furthermore, thanks to all the people from university who supported me in any way to finish my project and to my colleagues who created a fantastic working atmosphere in our office.

Special thanks to my family and all my friends for their mental support through all the years of studying. Without your help and love this way would not have been possible for me to go. A part of my success is your success.
Achievements without appreciation are worthless. Therefore, last but not least, thanks to anybody who grants me my success and celebrates it appropriately.

Table of Contents

1 Introduction **1**

2 Theoretical aspects **2**
2.1 Fluidics - Flow of liquid . . . 2
2.1.1 Continuum assumption . . . 2
2.1.2 Governing equation - Navier-Stokes . . . 3
2.1.3 Laminar vs Turbulent flow - Reynolds number . . . 4
2.1.4 Mixture of different liquids - Diffusion . . . 5
2.1.5 Hydrodynamical manipulation of liquids . . . 6
2.2 Optics - Guiding of light . . . 7
2.2.1 Total reflection . . . 7
2.2.2 Propagation of light through a waveguide . . . 8
2.2.3 Evanescent field . . . 9

3 Device Fabrication **11**
3.1 Constitution of the final devices . . . 11
3.1.1 Structuring the Silicon wafer . . . 12
3.1.2 Deposition of the SU-8 layer . . . 12
3.1.3 Final process steps . . . 13
3.2 Sealing of the microfluidic channels . . . 14

4 Waveguide Shifter **15**
4.1 Concept and basic description . . . 15
4.2 Developed designs . . . 16
4.2.1 Design one - Simplest realization . . . 16
4.2.2 Design two - Advanced device . . . 17
4.2.3 Design three - Additional features integrated . . . 18
4.3 Simulation of the developed designs using COMSOL . . . 18
4.3.1 Simulation software COMSOL Multiphysics . . . 18
4.3.2 Simulation results . . . 19
4.4 Device considerations . . . 22
4.4.1 Optical path . . . 22
4.4.2 Positions of in- and outlets on the chip . . . 23
4.4.3 Merging of cladding and core . . . 23
4.4.4 Alignment of the pushing inlets . . . 24

4.4.5 Dimensions of the shifting channel . . . 25
4.4.6 Liquid outflow from the chip . . . 26
4.5 Layout of the final devices . . . 27
4.6 Measurements . . . 30
4.6.1 Experimental setup . . . 30
4.6.2 Measurement results . . . 31
4.7 Simulation versus Measurement . . . 37
4.7.1 Design one - Simplest realization . . . 38
4.7.2 Design two - Advanced device . . . 38
4.7.3 Design three - Additional features integrated . . . 41
4.8 Bottom line . . . 43

5 Fluorescence Sensor **44**
5.1 Concept and basic description . . . 44
5.2 Developed design . . . 46
5.3 Simulation of the developed design using COMSOL . . . 47
5.3.1 Simulation software COMSOL Multiphysics . . . 47
5.3.2 Simulation results . . . 47
5.4 Device considerations . . . 48
5.4.1 Optical path . . . 48
5.4.2 Positions of in- and outlets . . . 49
5.4.3 Merging of core, sample and cladding . . . 49
5.4.4 Liquid outflow from the chip . . . 50
5.5 Layout of the final device . . . 51
5.6 Measurements . . . 52
5.6.1 Experimental setup . . . 52
5.6.2 Measurement results . . . 52
5.6.3 Sample width analysis . . . 55
5.7 First Conclusion . . . 57
5.8 Improved devices . . . 57
5.8.1 Design ideas . . . 57
5.8.2 Fabricated devices . . . 59
5.9 Bottom line . . . 62

6 Discussion and Conclusion **63**
6.1 Waveguide shifter . . . 63
6.2 Fluorescence sensor . . . 64
6.3 Overall conclusions . . . 65
6.4 Outlook . . . 65

A Mask layouts **66**
A.1 Wafer one . . . 66
A.2 Wafer two . . . 68

Literature **70**

1 Introduction

The importance of optofluidic micro-systems has increased enormously during the last years. Such systems are used for tasks in different application areas. Fields of application are medicine, biotechnology and optics. Although optofluidic micro-systems offer promising application possibilities, they are still in the development state and are not integrated in commercially available devices at the moment.

Liquid-core/liquid-cladding waveguides (L^2-waveguides) have both core and cladding of a waveguide provided in liquid form. Such waveguides offer similar properties as commonly available glass fibers, which is in fact low-loss transmission of light pulses. Additionally, the structure of L^2-waveguides can be redefined easily during operation which is impossible for glass fibers. This offers the possibility of adapting the core diameter of a waveguide to different wavelengths and still ensure low-loss transmission of the light.
Therefore, perfect conditions for light guiding can be achieved with the same L^2-waveguide for any light source by adaption of the waveguide dimensions.

In this work the development of two microfluidic systems which are based on L^2-waveguides is presented. The first one is a waveguide shifter. For this application hydrodynamical manipulations of liquids are used to steer an L^2-waveguide in a micro channel to define distinct outlet positions for the guided light.
The second system is in the field of analyzing applications. It takes use out of the evanescent field arising from an L^2-waveguide to excite fluorescent sample media. Compared to previous works [LWL$^+$08] the design of this fluorescence sensor was improved to enable different analyzing situations by simple velocity changes.

This written work is basically split into four parts. In chapter 2 the theory behind the phenomena appearing in this field of research is explained. Chapter 3 is about the fabrication process of the presented devices. Chapter 4 and 5 give the whole development process of the waveguide shifter and the fluorescence sensor, respectively. Both the waveguide shifter and the fluorescence sensor include a simulation part and the final measurements plus discussions.

2 Theoretical aspects

The devices described in this work are placed in two main regimes, fluidics and optics. Both of these fields are essential for the functionality of the developed designs. Another fact which has to be considered is the size of the devices which is in the micro-scale. Different phenomena occurs in this scale compared to the macro-world.
The following paragraphs give the theoretical background behind the investigated designs. Similar descriptions can be found in [Pär07].

2.1 Fluidics - Flow of liquid

Since all the developed devices in this paper are placed in the field of microfluidics the flow of liquid is of importance for all following applications. In the next sections the main phenomena and assumptions behind it are explained shortly.

2.1.1 Continuum assumption

Different phenomena occur while handling liquids. To describe the properties in the macro-scale models based on the continuum assumption can be used. Using a continuum is describable as an averaging process.
Figure 2.1 illustrates the continuum assumption for the density of a sample volume.

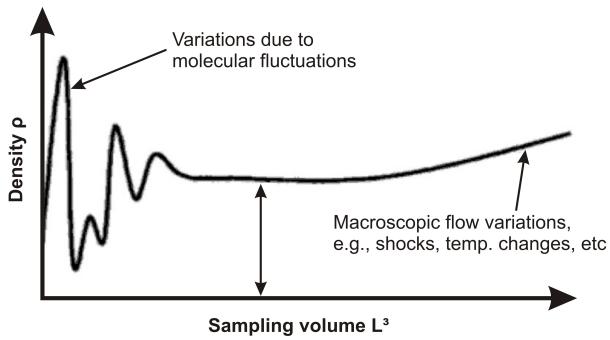

Figure 2.1: Continuum assumption in fluids illustrated by thought experiment for measuring density [NW02]

Having just a small sampling volume results in fluctuations of the density. After a certain amount of sample volume the density stays constant. A further increase results in variations due to macroscopic flow effects.
Therefore, a certain total amount of sample volume has to exist. If the amount gets too small the continuum assumption is not valid anymore.
The continuum assumption assumes that all quantities of interest (e.g. density, velocity, acceleration) are defined everywhere in space and vary continuously.

Liquids in the micro-scale

Before applying the continuum assumption it has to be ensured that it is still valid for the used dimensions. Referring to [NW02] a length scale of 10nm is the lower limit. Smaller dimensions cannot be described anymore by using this assumption.
The devices presented in here have much larger length scales. Therefore, the continuum assumption is suitable to describe these situations.

2.1.2 Governing equation - Navier-Stokes

The Navier-Stokes equations are the governing equations of a microfluidic system. Based on the continuum assumption the thermodynamic flow of liquid can be explained by these equations. When considering the flow of an incompressible, Newtonian, isotropic, Fourier conducting fluid these equations can be simplified as follows:

$$\frac{\partial u_i}{\partial x_i}(\rho u_i) = 0 \tag{2.1}$$

$$\rho\left(\frac{\partial u_i}{\partial t} + u_j\frac{\partial u_i}{\partial x_j}\right) = \rho\mathbf{F}_i - \frac{\partial p}{\partial x_i} + \frac{\partial}{\partial x_i}\left[\eta\left(\frac{\partial u_i}{\partial x_j} + \frac{\partial u_j}{\partial x_i}\right)\right] \tag{2.2}$$

$$\rho c_v\left(\frac{\partial T}{\partial t} + u_i\frac{\partial T}{\partial x_i}\right) = \frac{\partial}{\partial x_i}\left(\kappa\frac{\partial T}{\partial x_i}\right) \tag{2.3}$$

In these equations u_i represents the flow velocity, ρ the local density, p the pressure, F the body force, η the dynamic viscosity and c_v a specific heat at a constant volume. The repeated indices in any single term indicates a summation according to the accepted practice in index notation (Einstein summation convention)[NW02].

Equation 2.1 is called the continuity equation, 2.2 the momentum equation and 2.3 the energy equation. Assuming the flow remains at a constant temperature, (no temperature change is expected on the whole chip) these three equations can be further simplified to:

$$\frac{\partial u_i}{\partial x_i}(\rho u_i) = 0 \tag{2.4}$$

$$\rho\left(\frac{\partial u_i}{\partial t} + u_j\frac{\partial u_i}{\partial x_j}\right) = \rho\mathbf{F}_i - \frac{\partial p}{\partial x_i} + \eta\frac{\partial^2 u_i}{\partial^2 x_j} \tag{2.5}$$

Loose and Hess [LH89] showed an other situation where the validity of these equations breaks down. They showed that proportionality between stress and strain rate (Newtonian assumption) breaks down when using too high flow velocities in a channel. Together with the Newtonian assumption also the Navier-Stokes equations are not valid in such a situation. Since this breakdown velocity was determined to be about 10^6 m/s it has not to be considered for the velocities used in this work.

2.1.3 Laminar vs Turbulent flow - Reynolds number

For applications similar to these described in here (long straight channels of constant cross section) the Reynolds number can be used as a good predictor for determining if turbulence will occur. The Reynolds number is defined as follows:

$$Re = \frac{\rho D_h u}{\eta} = \frac{D_h u}{\nu} \tag{2.6}$$

D_h is the hydraulic diameter of the structure, u is the characteristic velocity in the channel, ρ is the density of the used fluid, η is the dynamic viscosity and ν the kinematic viscosity.
The hydraulic diameter D_h of the structure has to be determined before calculating the Reynolds number. It can be seen as a calculation of an equivalent diameter for non-circular channels.

$$D_h = \frac{4 * CrosssectionArea}{WettedPerimeter} \tag{2.7}$$

For channels which are entirely filled with liquid the $WettedPerimeter$ is simply given by the perimeter of the whole channel.

The transitional Reynolds number, the value where laminar flow turns over to turbulent flow, was found out to be between 1000 and 2000. It depends on many factors such as channel shape, aspect ratio, surface roughness, ..., so it cannot be determined generally. Below this number laminar flow is expected and above turbulent flow does occur.
For every pressure driven flow, which is the type of flow investigated in this work, a parabolic flow profile is expected. If turbulent flow appears the parabolic flow profile in a channel is not parabolic anymore.

In the later on presented devices the dimensions of the cross section of the channels are going to be below $400\mu m$ x $100\mu m$.
The hydraulic diameter is therefore calculated to be less than

$$D_h = 4 * \frac{100\mu m * 400\mu m}{1000\mu m} = 16 * 10^{-5} m. \tag{2.8}$$

Mostly DI (deionized) water is going to be used during measurements. DI water has a density of $1000 kg/m^3$ and a viscosity of approximately $9 * 10^{-4} Pa \cdot s$ at room temperature (25°C).
The investigated velocities are below $0.05 m/s$. So the maximum Reynolds number can be calculated to

$$Re = \frac{10^3 kg/m^3 * 16 * 10^{-5} m * 0,05 m/s}{9 * 10^{-4} kg/ms} \simeq 9. \tag{2.9}$$

This number is far below the above mention 1000-2000. So in all the following investigations laminar flow can be expected.

2.1.4 Mixture of different liquids - Diffusion

Another interesting phenomenon appearing while handling more than one fluid is diffusion.
In a liquid there is an agitation of the molecules due to temperature. If one molecule collides with another one it is deflected from its movement on a straight line. These deflections result in a mixture of liquids which are in contact to each other. This effect is called diffusion.

Using Fick's law, expressed as

$$J = -D\nabla c \tag{2.10}$$

diffusion can be described mathematically by using following differential equation:

$$\frac{\partial c}{\partial t} = div\,(D\nabla c) + S \tag{2.11}$$

Where J represents the mass flux of substance through a surface, D is the diffusion constant, c the concentration of molecules in the sample and S a source or sink term of concentration.
Figure 2.2 depicts the flux of substance J through an elementary surface δA.

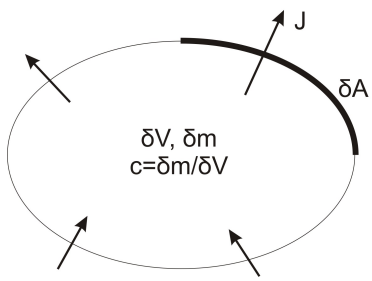

Figure 2.2: Schematization of an elementary volume with concentration c of diffusing substance [BS06]

As seen in figure 2.2 the concentration is given by

$$c = \frac{\delta m}{\delta V} \tag{2.12}$$

where δm is the mass and δV an elementary volume.

Skipping the derivation, the diffusion constant is given by

$$D = \frac{k_B T}{C_D}. \tag{2.13}$$

In equation 2.13 k_B represents the Boltzmann constant, T the temperature and C_D the friction factor.
Assuming the diffusion constant to be constant in a subdomain, independent from the spatial coordinates, equation 2.11 can be simplified to

$$\frac{\partial c}{\partial t} = D\Delta c + S. \tag{2.14}$$

This approach is just one out of more. It was decided to be the easiest for understanding the basics behind diffusion. For more information and different approaches the listed references can be used [BS06, ZT00].

2.1.5 Hydrodynamical manipulation of liquids

An expression which will be used several times in this thesis is hydrodynamical focusing, shifting or generally manipulation of liquids.
Figure 2.3 shows an application where hydrodynamical manipulations of liquids are used.

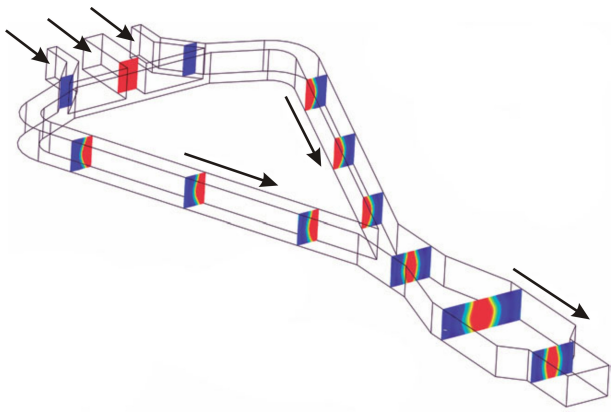

Figure 2.3: Hydrodynamically adjustable optofluidic microlens developed at the Technical University of Vienna [RV09]

Above shown design was developed to create a three dimensional liquid lens in the microscale. Two different liquids are used. One is colored red in the picture and the other one blue.
The liquids are brought in on the left side and sandwiched shortly after the inlet. By having curved channel designs the parabolic flow profile in the channel is used to obtain two half-lens-like structures visible in the middle of figure 2.3. Joining these two half-lens-like profiles and enlarging the channel after the junction results in a three dimensional lens structure.

By setting the inlet velocity for the blue liquid to a higher level you can hydrodynamically compress the red liquid and obtain a smaller lens structure at the end. Decreasing the velocity of the blue liquid results in a broadening of the red liquid and finally a bigger lens shape is obtained at the outlet.

All these manipulations of liquids mentioned above are hydrodynamic. Treatments similar to these are used later in this work to fulfill certain applications.

2.2 Optics - Guiding of light

For this work guiding of light is of same interest as the flow of liquid. Since all devices are opto-fluidic micro-systems, optics play an important rule to fully understand the working functionality of these devices.

2.2.1 Total reflection

The phenomenon used for guiding of light with little losses through a certain waveguide is the total reflection of light.

We start from the equation for an incident plane wave between two dielectric materials, (i) and (t), with indices of refraction n_i and n_t, respectively.

$$\mathbf{E}^i = \mathbf{E}_0^i e^{-j\left(\mathbf{k}^i \cdot \mathbf{x} - \omega t\right)} \tag{2.15}$$

Where $\mathbf{E}$ stands for the electric field and $\mathbf{k}$ for the wave vector.
By changing index i to r and t the equations for the reflected and the transmitted wave are obtained.

Directly at the interface between medium (i) and (t), so at $z = 0$, these three wave functions are given by:

$$\mathbf{E}^{i,r,t} = \mathbf{E}_0^{i,r,t} e^{-j\left(\mathbf{k}_{||}^{i,r,t} \cdot \mathbf{x} - \omega t\right)} \tag{2.16}$$

Where $\mathbf{k}_{||}^{i,r,t}$ stands for the projections of the wave vectors onto the interface.

Since the phase angle of these three waves, incoming, reflected and transmitted, has to be the same at the interface, equation 2.17 has to be fulfilled.

$$\mathbf{k}_{||}^i = \mathbf{k}_{||}^r = \mathbf{k}_{||}^t \tag{2.17}$$

Furthermore, the magnitudes of the wave vectors are given by

$$|\mathbf{k}^{i,r,t}| = k^{i,r,t} = n_{i,r,t} k_0. \tag{2.18}$$

Thus the wave vectors for the reflected and the transmitted wave are explicitly given.

If n_i is larger than n_t and the incidence angle of light Θ^i is big enough, as shown in figure 2.4, it can occur that the tangential component of the incoming wave vector from medium (i) is bigger than the magnitude of the wave vector in medium (t).
In such a situation no free plane wave exists in medium (t) and no light is transmitted into it. The whole light is reflected. This phenomenon is called total reflection.

Having given indices of refraction n_i and n_t the critical angle for total reflection can be calculated.

$$\Theta_{crit} = arcsin \frac{n_t}{n_i} \tag{2.19}$$

Total reflection is obtained if

$$\Theta^i > \theta_{crit}. \tag{2.20}$$

This derivation and more information can be found in [Rei05].

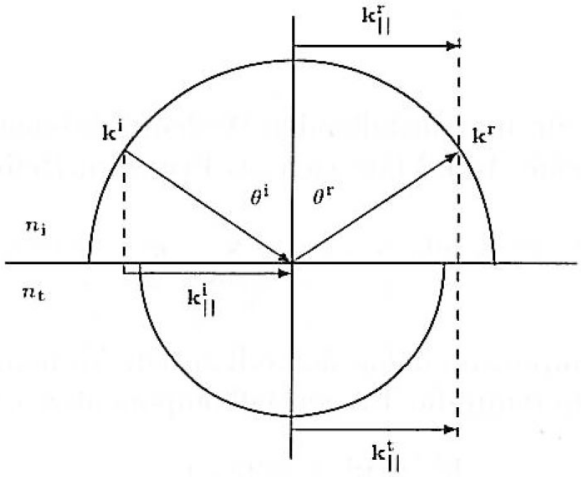

Figure 2.4: Total reflection explained by the phase angle condition for the wave vectors [Rei05]

2.2.2 Propagation of light through a waveguide

The phenomenon of total reflection at the interface between a medium with higher index of refraction and one with lower index is used to build up waveguide structures such as the planar waveguide shown in figure 2.5.

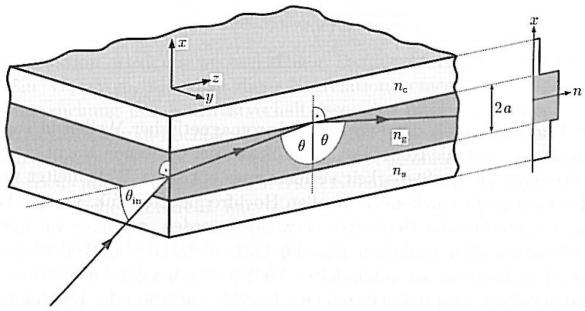

Figure 2.5: Planar waveguide structure [Rei05]

It consists out of three layers. One core layer sandwiched between two cladding layers. The core layer, n_g, is provided as a medium with higher index of refraction than the two cladding layers, n_c and n_s. In most waveguides n_c and n_s are chosen the same. Therefore, it is assumed in the following sections that $n_c = n_s$.
If the angle Θ_{in} is chosen small enough, total reflection will occur inside the planar waveguide and the light is guided through the waveguide with minimum losses.

The maximum of Θ_{in} to still provide total reflexion is defined by the numerical aperture NA.

$$\Theta_{in} < n_g\sqrt{1 - sin^2\Theta_{crit}} = \sqrt{n_g^2 - n_s^2} =: NA \tag{2.21}$$

Any angle below NA results in guiding of light through the structure with minimum losses.

In the devices described later on a structure similar to figure 2.5 is used. Special for the realization are core and cladding media provided in liquid form.

2.2.3 Evanescent field

In the section before it was spoken about guiding light with a minimum of losses if total reflection in a waveguide is obtained. This obviously leads to the conclusion that there certainly are losses of light. These losses can be seen as light which escapes the core of a waveguide into the cladding of it. This escaped light is the evanescent field.

Figure 2.6 shows the first mode of the electric field in a waveguide consisting out of a core, illustrated gray on the figure, and two cladding regions on top and bottom of the core.

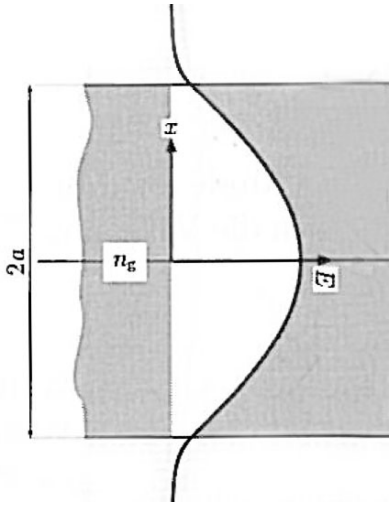

Figure 2.6: First mode of the electric field distribution in a planar waveguide [Rei05]

It can be seen that most of the intensity is guided in the core region. The shape of the mode can be described as a Gaussian distribution. On both contact regions, core-cladding, the tail of the Gaussian function reaches into the cladding medium. These tails are the evanescent field of the guided wave function.
Close to the core, $z = 0$, this field has its maximum and decreases continuously towards zero in the far field, $z = \infty$. Figure 2.7 depicts this circumstance.

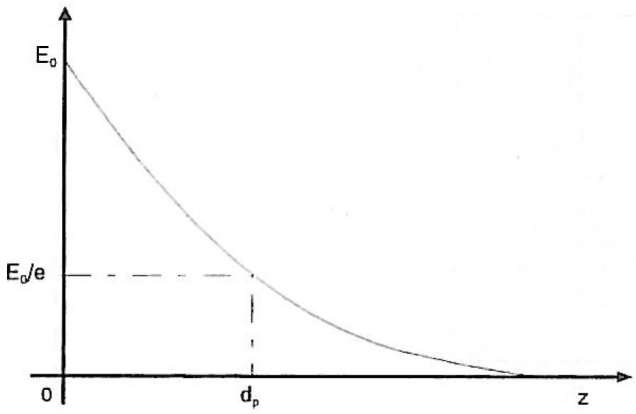

Figure 2.7: Evanescent field penetration into the cladding medium [For01]

On figure 2.7 E_0 stand for the magnitude of the electric field at the core-cladding interface. At

the point where the magnitude reaches E_0/e the penetration depth d_p of the evanescent field is defined.

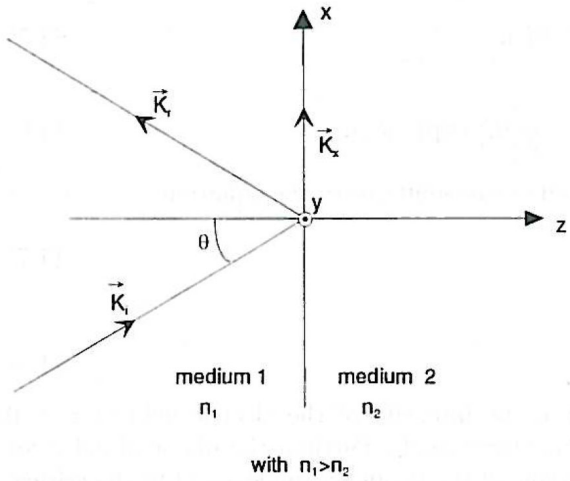

Figure 2.8: Geometry used for the calculation of the penetration depth [For01]

Using the geometry shown in figure 2.8 this penetration depth can be calculated using following equation:

$$d_p = \frac{\lambda}{2\pi\sqrt{{n_1}^2 sin^2\Theta - {n_2}^2}} \tag{2.22}$$

Where λ stands for the wavelength of the guided light, n_1 and n_2 for the indices of refraction of core and cladding and Θ for the incidence angle of the light.

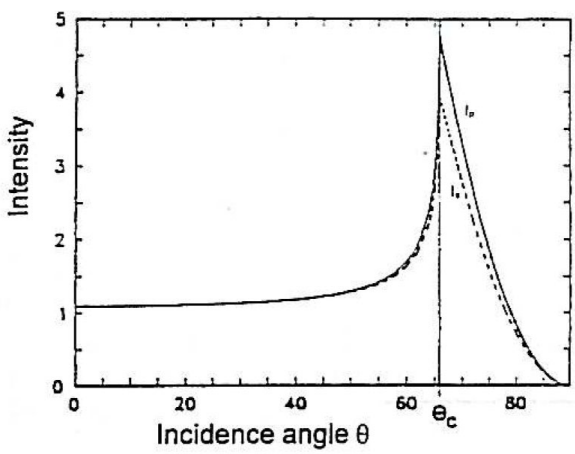

Figure 2.9: Electric field intensity at the interface depending on the incidence angle Θ [For01]

Figure 2.9 shows the magnitude of the electric field at $z = 0$ depending on the incidence angle Θ. There is a maximum when Θ reaches the critical angle for total reflection Θ_{crit}.

3 Device Fabrication

The fabrication of the devices was carried out in the clean room of the Institute of Sensor and Actuator System at the Technical University of Vienna. Peter Svasek, the main responsible person for fabrication, and his colleagues published several papers about SU-8 layer fabrication. One of these papers can be found in the given list of references [SSLV04].

3.1 Constitution of the final devices

Figure 3.1 depicts the different layers building up the final structure of the devices.

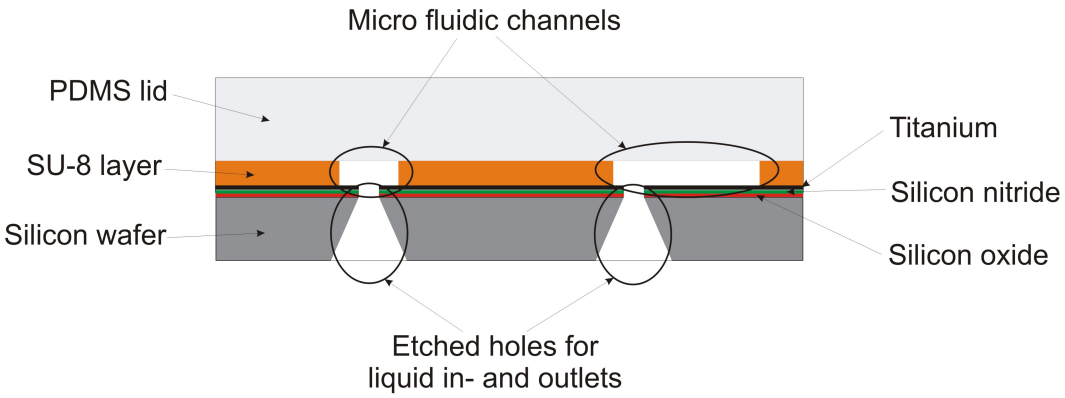

Figure 3.1: Schematic cross-section of a finally fabricated device

The chips basically consist out of three main layers:

- Silicon wafer, thickness: 350μm
- SU-8 layer, thickness: 100μm
- PDMS lid, thickness: 0.5-3mm

Between Silicon wafer and SU-8 layer a titanium layer, a film of silicon nitride (70 nm) and one of silicon oxide (150 nm) are sandwiched. The titanium layer with a thickness of 100 nm is used for better adhesion of the SU-layer. The silicon oxide and nitride are essential for deposition of the SU-8 layer.

3.1.1 Structuring the Silicon wafer

The first fabrication step is etching the desired holes through the silicon wafer.
Before doing that the silicon oxide and silicon nitride film, which is placed on both sides of the wafer for protection reasons, is removed from one side by reactive ion etching (RIE). After removing the protection layer, the actual structuring process is done. This process comprises following steps:

- Spin coating of standard photo resin (AZ6612) onto the whole wafer with a rotation speed of 4000 rotations per minute.
- Curing of the photo resin on a hot-plate with 100°C for 5 minutes.
- Exposure of the resin through the desired mask (see appendix) for 5 seconds.
- Development of the resin by immersion of the whole wafer into a standard developer (AZ826) for 12 seconds.
- Etching of the holes with a 40% KOH solution. This process takes 6 hours and 20 minutes. The silicon oxide and silicon nitride films are used as an etch-stop.
- Removal of the remaining photo resin from the wafer.

After these steps a structure as shown in figure 3.2 is obtained.

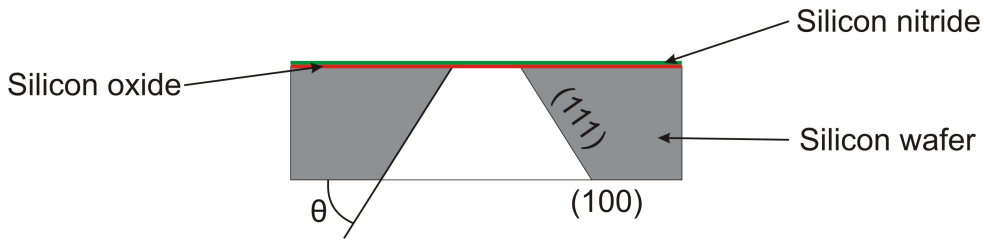

Figure 3.2: Etched holes illustrated schematically

Since etching silicon with KOH is an anisotropic etching method, the etch rate in [100]-direction is much higher than in [111]-direction, the walls of the etched holes are sloped as shown in figure 3.2. The angle Θ is 54.74°.
The silicon oxide (illustrated red) and nitride (illustrated green) layers on top of the wafer are essential for the next processing step.

3.1.2 Deposition of the SU-8 layer

After etching holes through the silicon wafer the SU-8 layer is deposited on it. For this process step it is essential to have a flat surface. This is provided by the silicon oxide and silicon nitride layers on top of the wafer. Without these layers spin coating of SU-8 onto the wafer would not be possible. The following steps are needed to obtain an SU-8 layer of 100μm thickness:

- Evaporation deposition of a 100nm titanium layer to provide excellent adhesion of the SU-8 layer on the silicon wafer.

- Spin coating of the first SU-8 layer onto the wafer by applying a rotation speed of 500 rotations per minute for 8 seconds.
- Equal dispersion of SU-8 on the whole chip by rotating the wafer at 2000 rotations per minute for 40 seconds.
- Curing of the first SU-8 layer on a hot-plate with 95°C for 30 minutes.
- Spin coating of the second SU-8 layer onto the wafer by applying a rotation speed of 500 rotations per minute for 8 seconds.
- Equal dispersion of SU-8 on the whole chip by rotating the wafer at 1800 rotations per minute for 40 seconds.
- Curing of the second SU-8 layer on a hot-plate with 95°C for 50 minutes.

After these process steps an SU-8 layer of approximately 100μm thickness is achieved.
For structuring the SU-8 layer more fabrication steps are necessary:

- Exposure of the SU-8 layer for 60 seconds.
- Post exposure bake for 20 hours on a hot-plate at 60°C.
- Development of the structures by use of a standard dissolver (PGMEA) for 8 minutes.
- Hard bake of the final device for 1 hour on a hot-plate at 160°C.

After all these steps SU-8 structures with high quality are obtained.

3.1.3 Final process steps

Before cutting the wafer into small chips a few last steps have to be done:

- The silicon oxide and silicon nitride membranes which are present between the SU-8 structures and the etched holes through the silicon wafer, are removed by using a Mega-sonic cleaner which couples an acoustic 1 MHz signal into a normal water beam.
- Spray coating of a standard photo resin (AZ4562) onto the wafer for protection reasons.
- Cutting the wafer by use of Discodad3220 at a saw-blade rotation speed of 4000 rotations per minute.
- Removal of the photo resin with included sawing-dust by use of a 5% KOH solution.

After all the previously explained processing steps structures like shown on figure 3.3 can be obtained. Aspect ratios of more than 20 are easily achievable.

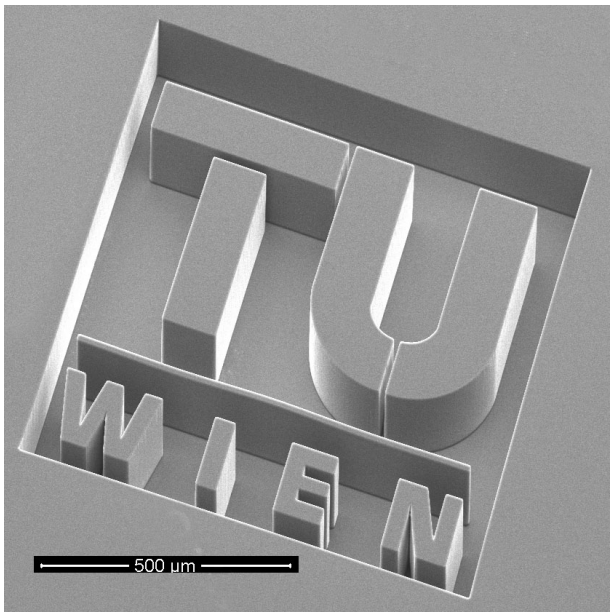

Figure 3.3: SEM image of a fabricated SU-8 structure

3.2 Sealing of the microfluidic channels

After applying all necessary fabrication steps three dimensional structures are obtained. In this work these structures are micro channels used for guiding of liquid. All these channels have to be closed before starting the final application.
This is done by use of conventional Polydimethylsiloxane (PDMS) lids. They are taken as waterproof gasket sheets for closure of the microfluidic channels. Different thicknesses of these lids are used. They are in the range of 0.5-3mm.

4 Waveguide Shifter

The principle of this waveguide shifter is based on liquid core liquid cladding waveguides, L^2-waveguides. For such waveguides both cladding and core are provided in liquid form. As necessary for commonly available glass-fibers and also for L^2-waveguides the difference between the indices of refraction of cladding and core has to be sufficient to provide good light guiding. Several liquids fulfill this requirement. For this application a 5mol $CaCl_2$ per liter DI water solution was used as core medium and DI water was used as cladding. During research also other combinations of liquids were tested.

4.1 Concept and basic description

One of the first requirements for an L^2-waveguide-shifter is guiding the light without too much losses. Therefore, proper core and cladding media need to be applied. The final design has to have at least inlets for core and cladding fluids.

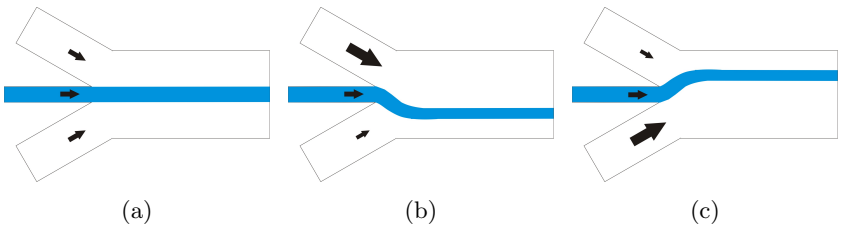

Figure 4.1: Schematic of the first design-idea and the principle working function

With a set-up shown in figure 4.1 it is possible to guide light straight through the chip (4.1(a)) and, by choosing different inlet-velocities for the upper and the lower cladding, you could even steer the light downwards (4.1(b)) and upwards (4.1(c)). The blue line on the images should depict the core fluid. The size of the arrows, drawn in the figures, should be seen in relation to the inlet velocity. Bigger arrow means higher inlet velocity.

Unfortunately, steering by using different cladding velocities does not cause big shifting of the core stream. Therefore, in an improved design idea, five inlets are provided. One inlet is still

used for the core medium. Two inlets on both sides of the core are used for the cladding and two other inlets are used to push the whole L^2-waveguide upwards and downwards.

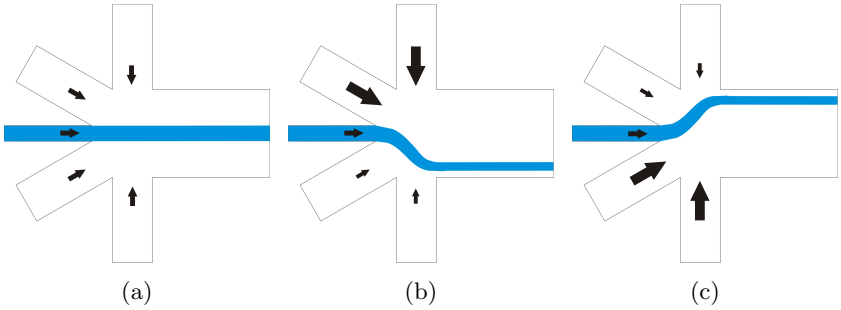

Figure 4.2: Schematic of the final design-idea and the principle working function

Figure 4.2 shows the schematic and principle working function of the final design. For sufficient light guiding core and cladding inlets are provided as in the first design idea already. To improve the ability of waveguide shifting two pushing inlets are placed on top and bottom of the waveguide. This increases the possibility to push the core downwards (4.2(b)) and upwards (4.2(c)). This principle setup configuration will be used in every following design. They differ in several details but all of them contain these five inlets for core, cladding and pushing fluids.

4.2 Developed designs

Three different designs were developed to investigate L^2-waveguide shifting. All three designs have one common detail. The read-out was decided to be done visually. I.e. the out coming light beam is visualized in a fluorescent medium. Therefore, arranged close to the end of the waveguide shifter, a pool will be placed on every chip. The light which exits the design has to go through that pool. Since it is expected to be filled with a fluorescent medium sensible in the range of the shifted light, the out coming light excites fluorescence and the beam is visualized. In the next sections only the real waveguide shifter part of the chips will be discussed. The read-out is described in a later part of this work.

4.2.1 Design one - Simplest realization

The first design was tried to be kept as simple as possible. No "special features" are integrated. With such a design the basic principle should be shown. As explained in the previous section five inlets are provided. Core and cladding inlets are placed next to each other. As necessary for good waveguide performance, the angle between them is kept small to create a smooth core-cladding contact region. The two pushing inlets are arranged perpendicularly to the core inlet.
Figure 4.3 shows the layout drawn in COMSOL 3.5 for the first chip-design. The channel width in the middle of the design, i.e. the region where the L^2-waveguide should be finally shifted, is 714 μm. For further dimension check the Bricscad-drawing (4.15(a)) of this design.

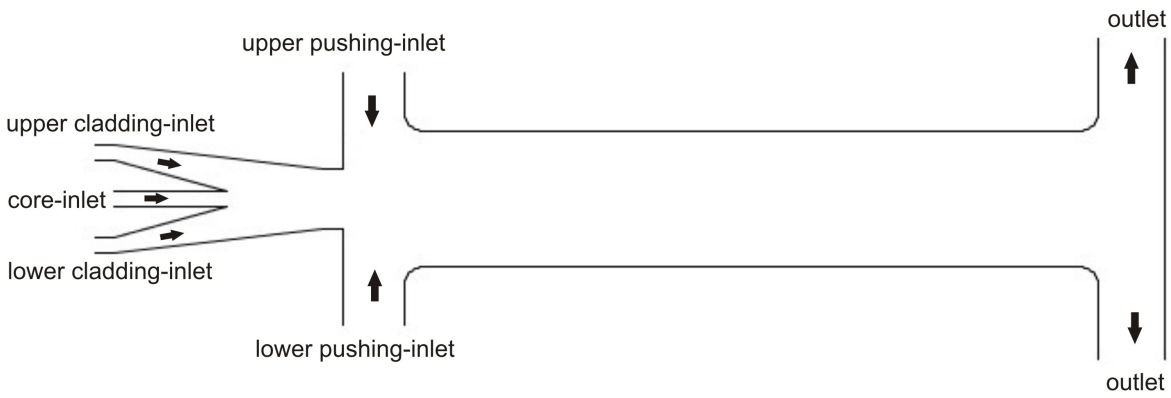

Figure 4.3: Simplest design to show waveguide shifter functionality

4.2.2 Design two - Advanced device

In a next development step the design was tried to be slightly improved. Since it was observed in preceding measurements that perpendicular inlets, like the pushing inlets in design one, are disadvantageous for gas-bubble-free liquid guiding, these were removed in this design and replaced by inlets arranged in a 45° angle with respect to the core inlet. With such sloped inlets flushing the whole channels with liquid to obtain a gas-bubble-free measurement situation is expected to be easier.
If two outlets exist another problem has been observed in preceding measurements. One of the outlets is always preferred. I.e. the liquid flows more likely through this outlet than through the other. As a second improvement, a tip was mounted in the middle of the outlet region. This should ensure that both outlets are used equally. The liquid should be split by the tip and guided to both outlets equally.

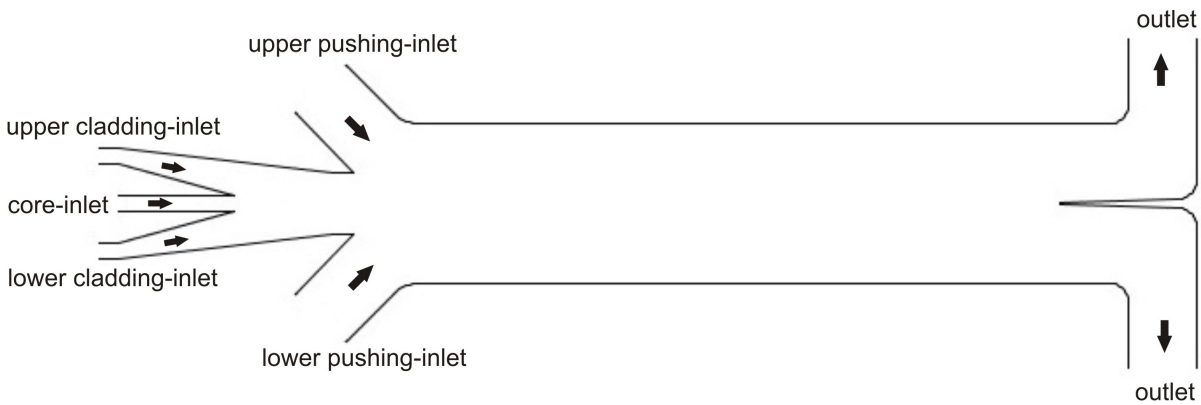

Figure 4.4: Second design with sloped pushing inlets and a tip placed in the middle of the outlet region

Figure 4.4 shows the COMSOL 3.5 drawing of the second design. The channel width in the middle of the design is 814μm. This information is given to get a feeling for the dimension of this design. To get more dimensions check the Bricscad file of this design (4.15(b)).

4.2.3 Design three - Additional features integrated

For the third design further adaptations were done. Similar to the second design a tip in the middle of the outlet region was implemented. Furthermore, two additional tips were placed to the left and to the right of the middle tip. This should fix the waveguide at this positions, define three distinct outlet positions for the light beam and stabilize the flow. Finally, the core which is flowing directly towards one of the two side-tips is expected to be split and turned sharply towards the nearest outlet after the tip. The light, which is guided in the core, should leave the core exactly at this position and a distinct outlet position for the light should be defined.

To increase the area of shifting the middle channel was enlarged conically. This should have an additional advantage also. Due to the enlargement of the channel the core will be enlarged too which should lead to better light guiding with less losses.

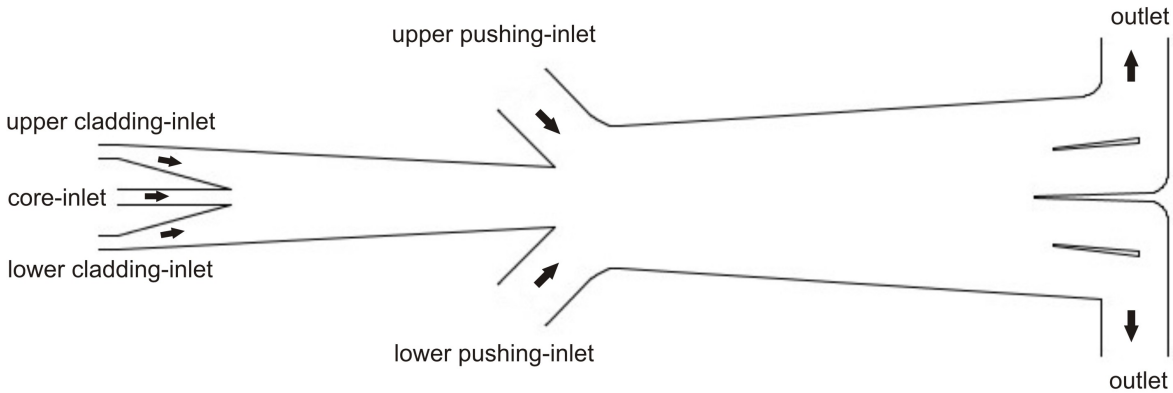

Figure 4.5: Third design: Two additional tips at the outlet and increasing shifting channel

Figure 4.5 shows the COMSOL 3.5 drawing of that design. The dimension of the shifting channel, placed in the middle of the chip, close to the outlets is 1080μm. For more dimensions check the Bricscad drawing of this design (4.15(c)).

4.3 Simulation of the developed designs using COMSOL

The estimation of the functionality of the designs before fabrication is an essential step during development. Therefore, to analyze the function of the designs, simulations were conducted before manufacturing. The simulation software COMSOL Multiphysics was used.

4.3.1 Simulation software COMSOL Multiphysics

COMSOL is a quite huge simulation software. It is based on finite element solving. It can be used for several different physical domains. Acoustic, magnetic, electric and several other situations can be simulated. Furthermore, these domains can be coupled and simulated with respect to each other.
For this work the flow of liquid is the domain of interest. As described in the theory section of this work the Navier-Stokes equations play an important rule for simulation. A second phenomenon

which has to be considered is diffusion. These two entities were simulated one after each other to estimate the working functionality of the developed designs.

4.3.2 Simulation results

In the next sections the simulations for all three designs will be shown. In all simulation results the red liquid stream should illustrate the core. The cladding and the pushing liquid are visualized in blue to highlight the core stream. In the contact region of core and cladding diffusion occurs and is visualized by a color gradation from red to blue.

4.3.2.1 Design one - Simplest realization

In order to ensure the ability of this design to shift the waveguide, simulations were done for three different outlet positions of the core. One in the middle of the channel, one in the upper part and one in the lower part.

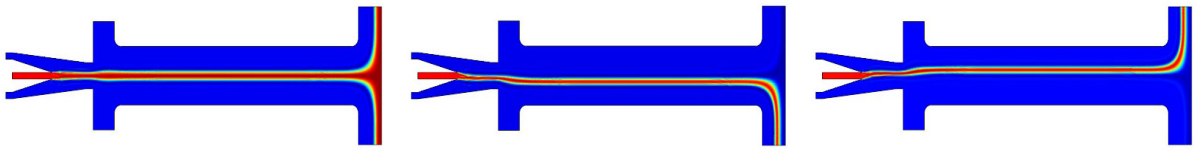

(a) (b) (c)

Figure 4.6: Simulation results for waveguide shifting for design one

To obtain the images shown in figure 4.6 the following inlet velocities have been chosen:

Simulation of hydrodynamical shifting - Design one			
Type of velocity	To the middle 4.6(a)	Downwards 4.6(b)	Upwards 4.6(c)
core velocity	6 μL/min	6 μL/min	6 μL/min
upper cladding velocity	6 μL/min	15 μL/min	8 μL/min
lower cladding velocity	6 μL/min	8 μL/min	15 μL/min
upper pushing velocity	6 μL/min	13 μL/min	6 μL/min
lower pushing velocity	6 μL/min	6 μL/min	13 μL/min

Table 4.1: Inlet velocities for simulations of hydrodynamical shifting as shown in figure 4.6

Figure 4.6(a) shows the situation where the light should leave the chip in the middle of the channel. Therefore, the inlet velocities where chosen to be the same.
For a situation in which the core flows directly in the middle of the channel, the core stream is expected to be split and guided equally to both outlets.

The next figure (4.6(b)) shows the situation where the waveguide is shifted downwards in the channel. Here the core stream is guided to the lower outlet entirely.

The third case is shifting the core to the upper part of the channel. This is shown in figure 4.6(c). Compared to shifting downwards the core liquid should leave the chip entirely through the upper outlet.

4.3.2.2 Design two - Advanced device

The next simulations were done for characterization of the second design. Similar to the previous section the cases for shifting the waveguide to the middle, upwards and downwards were simulated.

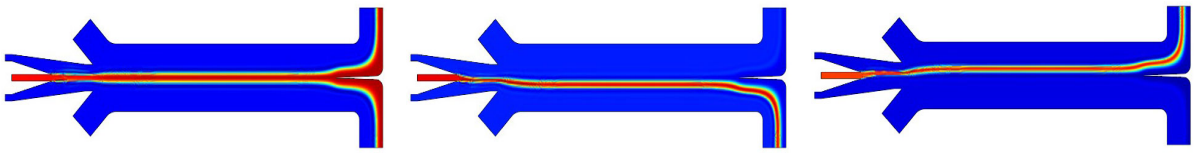

(a) (b) (c)

Figure 4.7: Simulation results for waveguide shifting for design two

To obtain the images shown in figure 4.7 the following inlet velocities have been chosen:

Simulation of hydrodynamical shifting - Design two			
Type of velocity	To the middle 4.7(a)	Downwards 4.7(b)	Upwards 4.7(c)
core velocity	6 μL/min	6 μL/min	6 μL/min
upper cladding velocity	6 μL/min	15 μL/min	8 μL/min
lower cladding velocity	6 μL/min	8 μL/min	15 μL/min
upper pushing velocity	6 μL/min	13 μL/min	6 μL/min
lower pushing velocity	6 μL/min	6 μL/min	13 μL/min

Table 4.2: Inlet velocities for simulations of hydrodynamical shifting as shown in figure 4.7

Figure 4.7(a) shows the case for shifting the waveguide towards the middle of the channel. All five inlet velocities were selected to be the same.
Similar to the first design the core liquid should leave the chip equally through both outlets. The only difference is the broadening of the core stream due to the tip mounted in the middle of the channel.

The next switching position is towards the lower part of the channel. This is shown in figure 4.7(b).

Expectedly, the core fluid leaves the design completely through the lower outlet.

The third case is shifting the core upwards. Figure 4.7(c) depicts this situation where the core stream is guided to the upper outlet entirely.

4.3.2.3 Design three - Additional features integrated

To estimate the functionality of the third design, similar to the two others, simulations for shifting the core towards the middle, downwards and upwards were done.

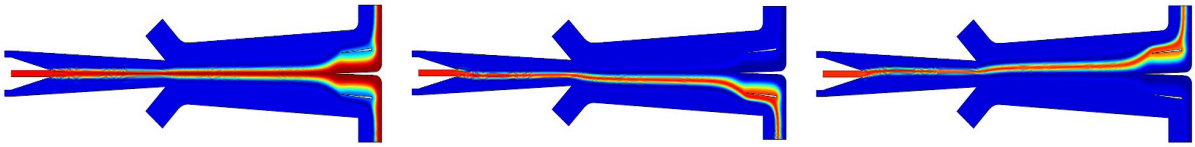

(a) (b) (c)

Figure 4.8: Simulation results for waveguide shifting for design three

To obtain the images shown in figure 4.8 the following inlet velocities have been chosen:

Simulation of hydrodynamical shifting - Design three			
Type of velocity	To the middle 4.8(a)	Downwards 4.8(b)	Upwards 4.8(c)
core velocity	6 μL/min	6 μL/min	6 μL/min
upper cladding velocity	6 μL/min	15 μL/min	8 μL/min
lower cladding velocity	6 μL/min	8 μL/min	15 μL/min
upper pushing velocity	6 μL/min	13 μL/min	6 μL/min
lower pushing velocity	6 μL/min	6 μL/min	13 μL/min

Table 4.3: Inlet velocities for simulations of hydrodynamical shifting as shown in figure 4.8

In figure 4.8(a) shifting towards the middle part of the channel is shown.
To obtain this result all inlet velocities were chosen to be 6μL/min.
It can be seen that, similar to the second design, the core is broadened due to the middle tip. Furthermore, it is visible that before reaching the tip the core is enlarged continuously. This is explained due to the conically broaden channel.

Next simulation was done for shifting the waveguide downwards in the channel (4.8(b)).
Similar to the two previous designs the core liquid should leave the chip entirely through the lower outlet. Additionally, it can be seen that due to the tip placed below the middle tip the core stream is fixed around this tip and turned sharply towards the outlet after it. This fact is meant to define a certain outlet position for the light.

The third case is shifting the waveguide upwards shown in figure 4.8(c).
As expected the occurring situation is similar to shifting the stream downwards just towards the upper outlet.

4.4 Device considerations

For the final fabrication of the device several components have to be investigated. Starting from the light source, guiding of light to the chip, guiding of light on the chip, up to placing of inlets, dimension of shifting area and outlets many parts have to be designed and fabricated sophisticatedly.

4.4.1 Optical path

For the final measurement set-up it is important to use a proper light source. In a previous section is was mentioned already that the read-out is planned to be done visually. Therefore, a pool filled with a fluorescent medium is used. Since this medium was decided to be Rhodamine B the wavelength of the light source has to be in the range of sensitivity of Rhodamine B.

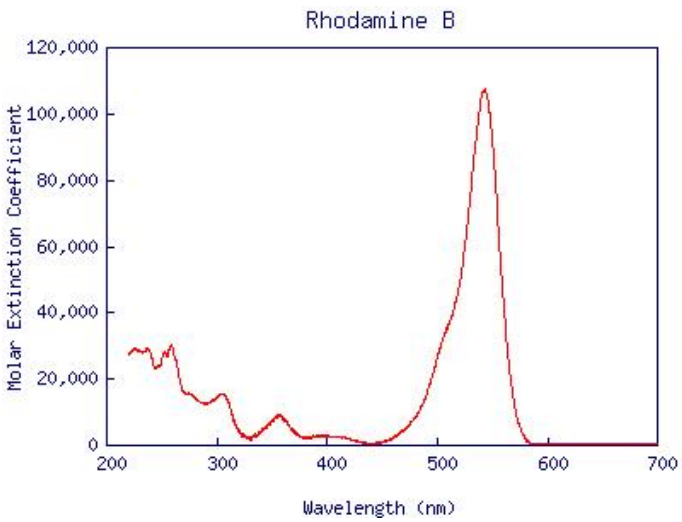

Figure 4.9: Absorption spectrum of Rhodamine B [DFL+98]

Figure 4.9 depicts the absorption spectrum of Rhodamine B. Since the maximum stays in between 520nm and 550nm the wavelength of the light source was chosen to be in the green region at about 530nm. The light source will be described more in detail in the measurement section of this chapter.

Another fact which is of importance for designing of the final devices is the diameter of the used glass fiber. This glass fiber is used to guide the light from the light source to the chip.
Two different glass fibers were available. One with a cladding diameter of 80μm and the other one with 120μm. For the final setup it was planned to use the 80μm glass fiber. To be able to use the 120μm glass fiber as well a special glass fiber inlet on the chip was designed. Figure 4.10

is an SEM (Scanning Electron Microscope) image of this special inlet.

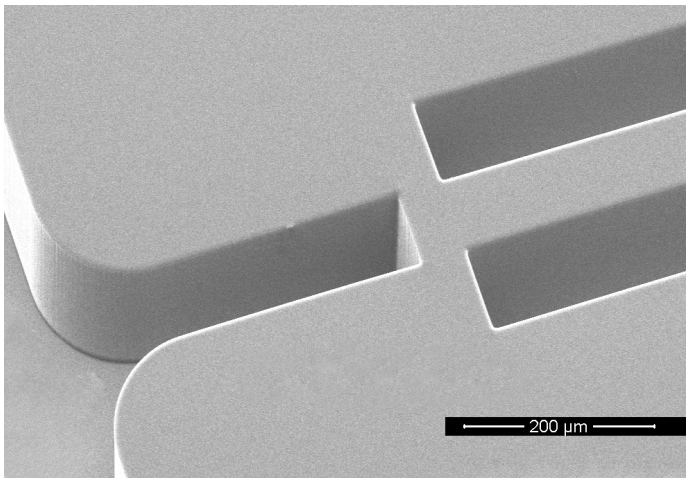

Figure 4.10: SEM image of the glass fiber inlet on the chip

On the left side it is enlarged to be able to bring in even thicker glass fibers. At the right side it narrows down to a width of 90μm. This was chosen for use of the 80μm glass fiber.

To obtain good results it is essential that most of the light is guided exactly towards the core inlet. In this case the maximum of light can be coupled into the liquid core.
To obtain straight light guiding towards the core inlet, a waveguide was constructed on the chip. The right side of figure 4.10 shows the beginning of this waveguide. The end is placed shortly before the core inlet which can be seen on the Bricscad drawings of the designs. In the middle of the waveguide, acting as core, an SU-8 bar is sandwiched between two layers out of air. Since the index of refraction of SU-8 ($n_{SU-8} \simeq 1.7$) is higher than of air ($n_{air} \simeq 1$) this design works as an integrated waveguide.

4.4.2 Positions of in- and outlets on the chip

A custom-made chip holder out of plastic is used to guid fluids into the chip. This holder consists out of a plastic block in which 3x4 holes are drilled-through on equally spaced positions. On the bottom of these holes tubings are connected which lead to syringes where the desired liquids can be filled in. Finally, on the other side of the holes the chip should be placed on. To provide excellent alignment of these 12 holes to the in- and outlets of the chip, it is essential that in- and outlets are placed just on these 12 positions. This fact has to be considered while designing the device. Figure 4.11 shows a picture of this custom-made holder.

4.4.3 Merging of cladding and core

The next important detail is the conjunction of core and cladding liquid. As discussed above the light is guided to the inlet of the core in a proper way. The next essential step is to ensure that just little losses occur between coupling of light into the core and merging with the

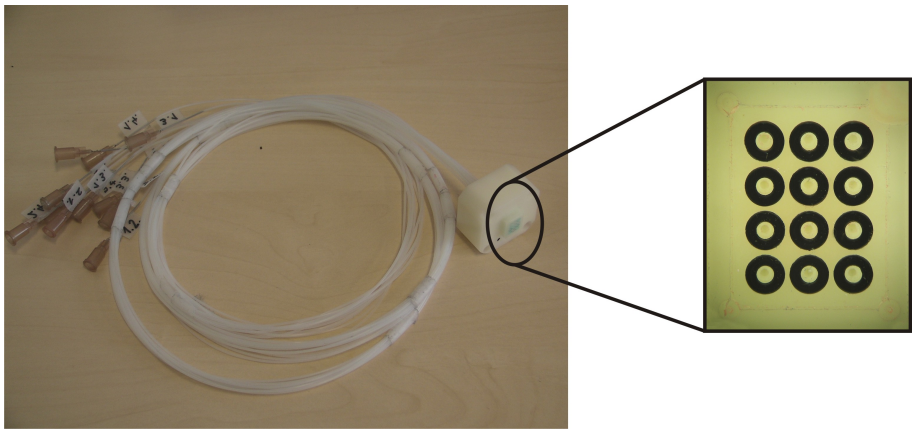

Figure 4.11: Custom-made chip holder

cladding. Therefore, this part of the channel, where the core liquid is not sandwiched in between the cladding medium, was tried to be designed as short as possible.

To provide a smooth merging of core and cladding fluid the angle between them has to be kept small. Choosing this angle to large would cause higher diffusion in the contact region, the light would not be guided well anymore and much higher losses would occur. Figure 4.12 shows an SEM-image of this part of the device.

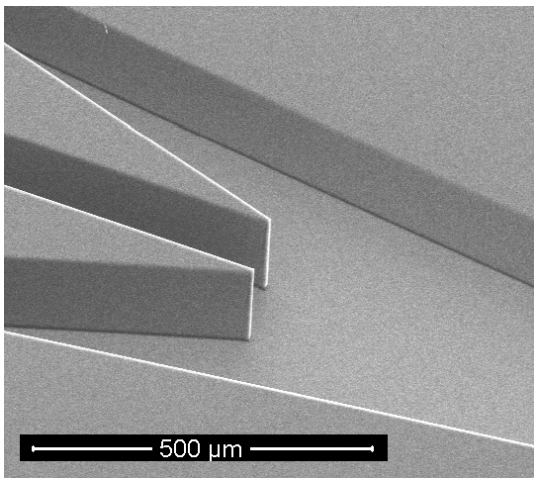

Figure 4.12: SEM image of the conjunction region of core and cladding

4.4.4 Alignment of the pushing inlets

There are several advisements about designing the pushing inlets. The first point is to decide at which point the pushing inlets should get in contact to the waveguide. It was chosen to place them shortly after the core-cladding merging. This should minimize space where no waveguide shifting takes place. I.e. the waveguide should turn up or down, as desired, more or less continuously. If there was too much place between core-cladding merging and pushing inlets, too much space

would be unused for the shifting process.
A second point concerns the angle between core inlet and pushing inlets. Angles from 20° to 90° were taken into account. Choosing the angle too small results in small shifting ability. Setting the angle to 90° results in higher diffusion and bigger gas-bubble problems.
Therefore, different designs were fabricated. One was designed with an angle of 90° and two others with an angle of 45° with respect to the core inlet.
These two kinds of pushing inlet alignments are shown in figure 4.13.

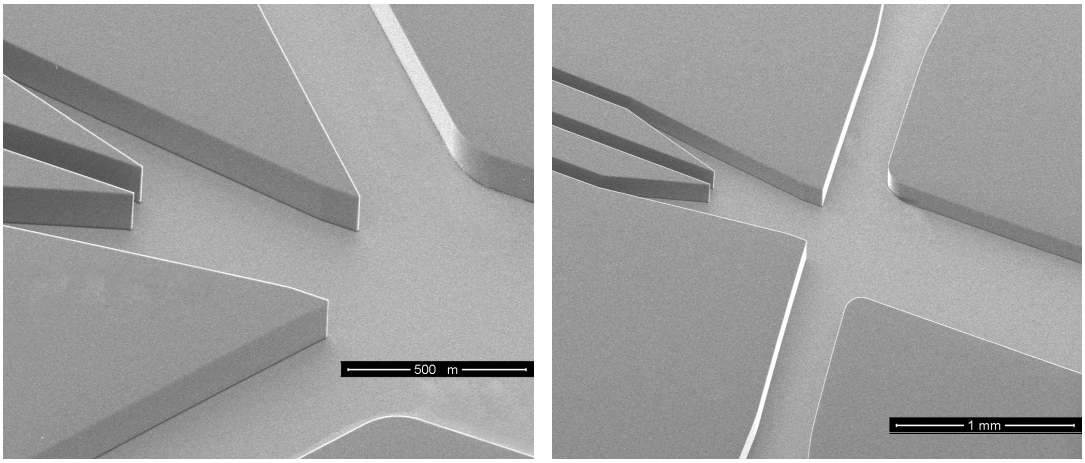

(a) (b)

Figure 4.13: SEM images of the different alignments of the pushing inlets

4.4.5 Dimensions of the shifting channel

Another important detail of the device is the shifting channel. I.e. the part of the device in which the waveguide moves upwards, downwards or stays in the middle.
Designing the channel walls parallel to each other or not is the first question to answer. Choosing a parallel assembly would result in a constant width of the core fluid. Increasing width of the channel would result in an increasing width of the core.
Both can be of interest. Increasing width of the core would yield better light guiding. Light which would escape the core normally would still stay within the core due to a core-enlargement. Parallel channel walls would yield better core confinement. If the core width does not increase you can reduce the core width at the outlet to a minimum.
To be able to test both of these design possibilities two different kinds of shifting channels were designed.

On figure 4.13 the beginning of the shifting channels and on figure 4.14 the end can be seen. It has to be imagined that one design is conically enlarged between the pushing inlets and the outlets and the other one keeps its width from the beginning to the end.

4.4.6 Liquid outflow from the chip

The last very important part of the devices will be the outlet. Obviously the fluid has to exit the chip again. It has to be decided how many outlets should be placed on the chip. To avoid unbalances due to more than one outlet it would be of advantage to have just one outlet for the whole chip. The final design is required to couple out light at the end of the chip at different positions. Just one outlet would not provide steering of the exiting light beam. All of the liquid, including the core, would flow out of the device at the same position and the light would leave the device on almost the same position for any inlet velocity.
Therefore, a device with two outlets was designed. They are arranged in a T-style. On figure 4.14 this part is shown.

Due to preceding measurements it is known that always one outlet is preferred if more than one outlet exists. In a T-style outlet always one of these two will be used more likely than the other.
For this reason a design was fabricated with a tip in the middle of the channel at the outlet. This tip should ensure that the liquid is split and guided to the two outlets equally.
Another idea was placing more than just one tip. In an advanced design three tips are provided at the outlet. The two side-tips should work as position fixers. When the core is split by one of these tips it should be fixed around it and turned sharply towards the nearest outlet after it. This sharp turn should provide good coupling out of light at this certain position.
Figure 4.14 shows the three different outlet regions which are used in the final designs.

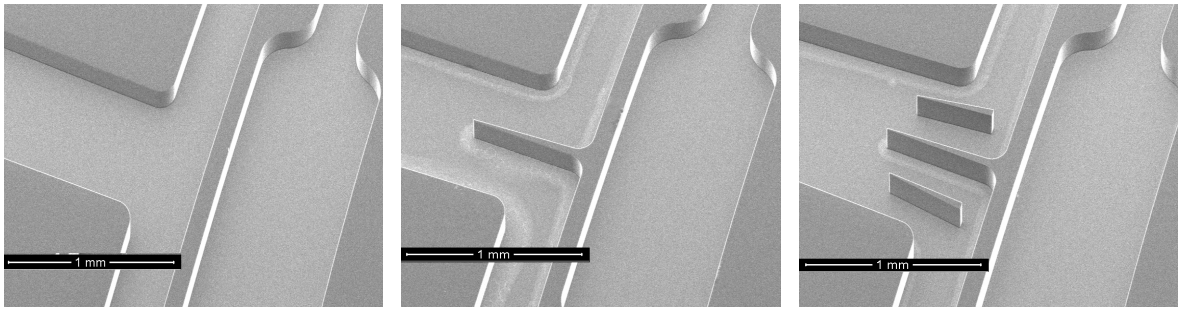

(a) (b) (c)

Figure 4.14: SEM images of the three different outlet-region designs which are used in the final designs

On the pictures also the Rhodamine pools used for the visual read-out are visible. They are placed close to the end of the shifting channel to minimize losses of light in the SU-8 bar between channel and pool.

4.5 Layout of the final devices

Three different designs were fabricated to investigate all the considerations explained above:

- Figure 4.15(a) and 4.16(a): The first device was tried to be kept as simple as possible. This design is expected to show the basic principle of waveguide shifting.
- Figure 4.15(b) and4.16(b): In an improvement the outlet region was changed slightly. A tip was placed in the middle to ensure equal use of both outlets. Furthermore, the pushing inlets were sloped and arranged in an angle of 45° with respect to the core inlet.
- Figure 4.15(c) and 4.16(c): The third design realizes all the ideas which were discussed above. Additionally to the tip in the middle of the outlet region two side-tips are placed on the chip. Furthermore, the shifting channel in the middle of the chip was enlarged towards the outlet.

See figure 4.15 for the CAD-files and figure 4.16 for images of the final devices.

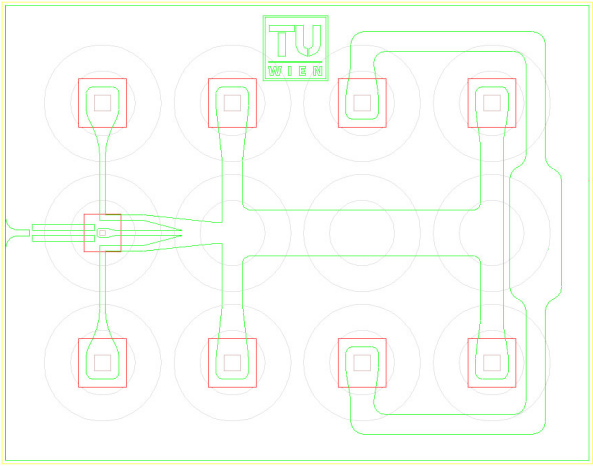

(a)

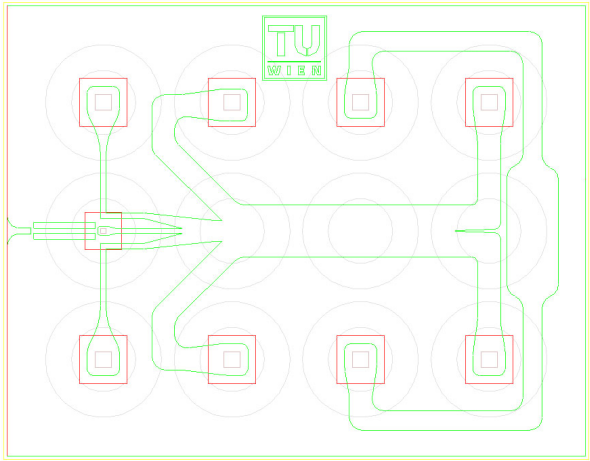

(b)

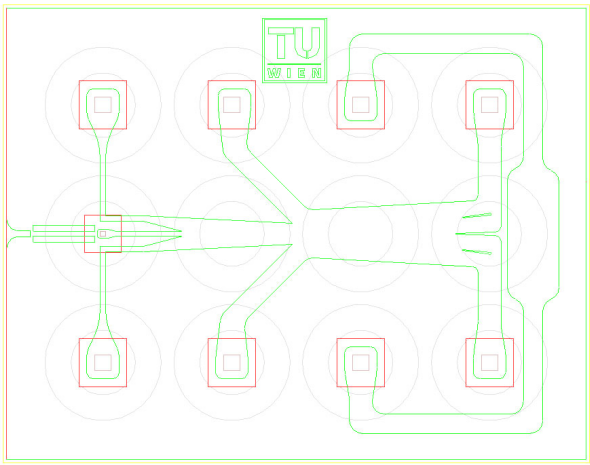

(c)

Figure 4.15: CAD-files of the three finally fabricated devices

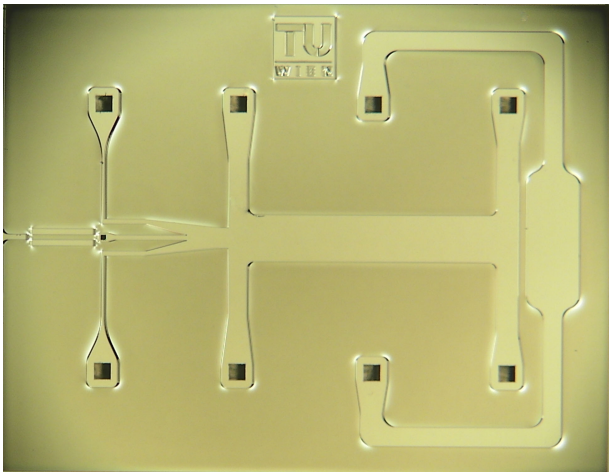

(a)

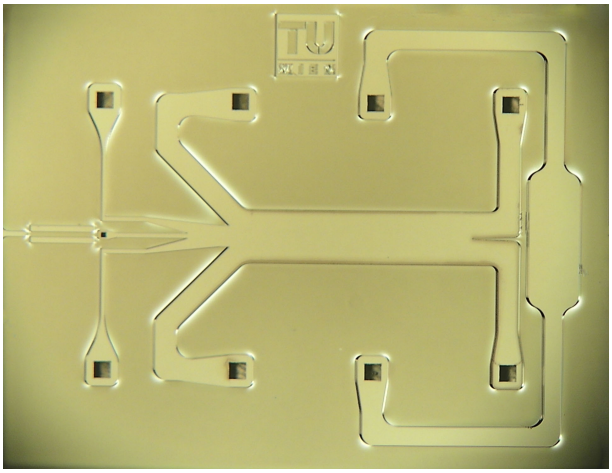

(b)

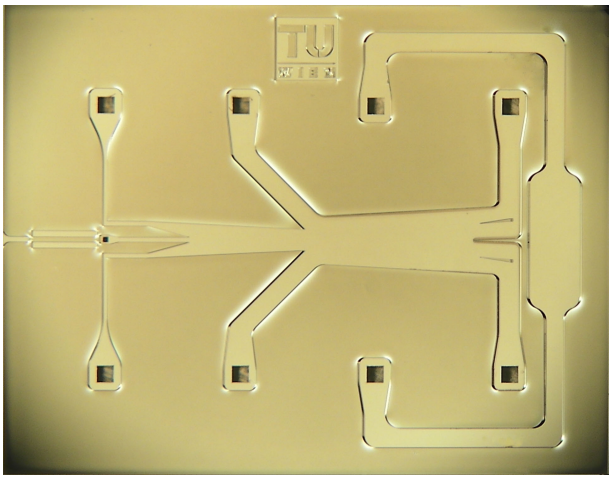

(c)

Figure 4.16: Images of the three finally fabricated devices

4.6 Measurements

4.6.1 Experimental setup

Figure 4.17 shows a sketch of the overall measurement setup. Syringe pumps were used to pump fluids into the chip. Depending on the measurements deionized water (DI water), colored DI water, an aqueous Rhodamine B solution, ethanol or a 5mol $CaCl_2$ per liter DI water solution was pumped into different inlets of the chip.

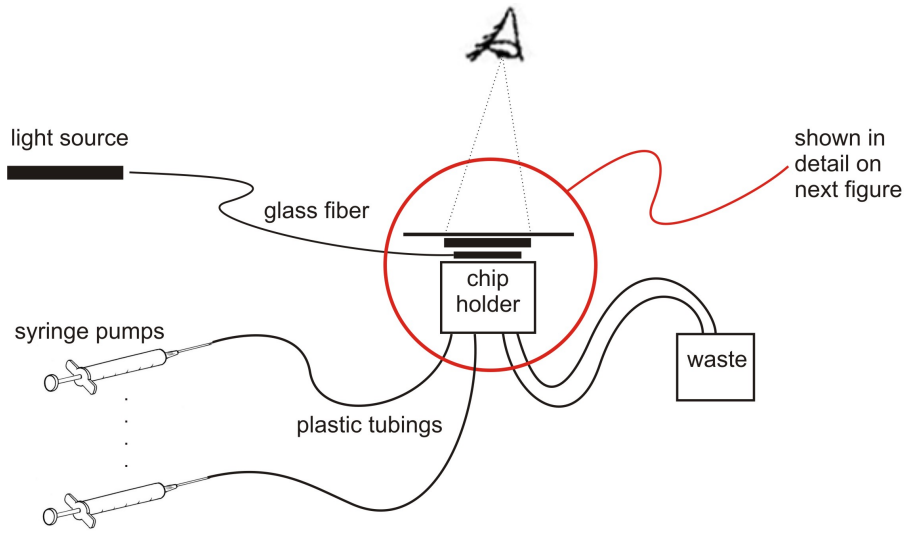

Figure 4.17: Sketch of the overall measurement setup used for characterization of the waveguide shifter devices

The fluids are guided in plastic tubings into the custom-made device holder with the chip placed on top of it. The holder and chip arrangement will be described in a later paragraph. The used liquids are guided into a waste box.
The light source was chosen to be a commonly available green laser pointer. The wavelength is 531nm and the output power is approximately 1mW.
Light was coupled into a glass fiber using a collimator. Both the collimator and the laser were placed on translation stages, movable in all three dimensions, to provide excellent alignment possibilities. Two different glass fibers were used during measuring. The diameters of the cladding were 80μm and 120μm.
The other side of the fiber is clamped into the prepared glass fiber inlet on the chip.

Figure 4.18 depicts the fixation of the chip onto the custom-made holder. As already mentioned in a previous section 3x4 holes are drilled-through the holder. The in- and outlets of the chip are designed directly at the positions of these 12 holes of the holder.
O-rings are placed between chip and holder to provided excellent sealing. To simplify fabrication the channel on the chips were compounded without cover. To close the channel and hence enable flow of liquid through the chip, a PDMS (Polydimethylsiloxane) layer was clamped on top of the chip.
The holder, including o-rings, chip and PDMS layer, is placed in a special setup which consists

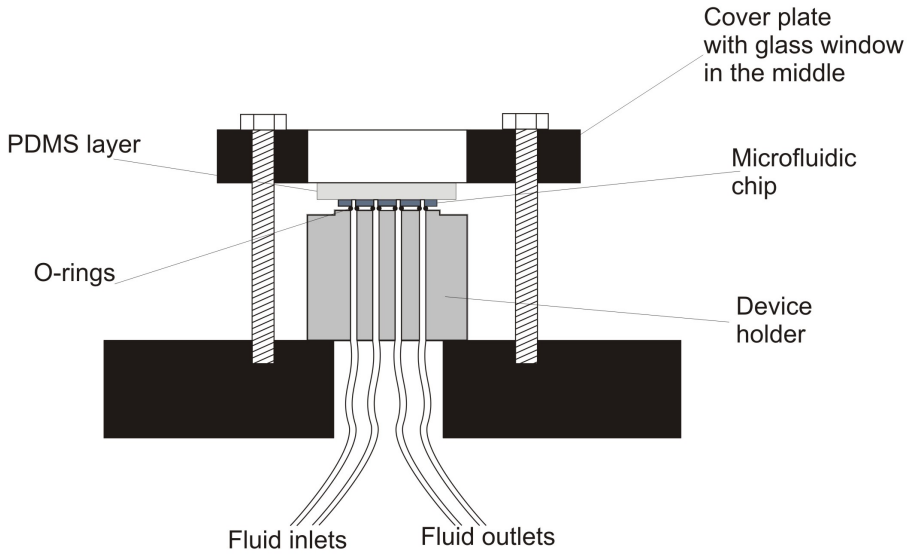

Figure 4.18: Cross-section of the fixation of the chip onto the custom-made holder

out of a cover plate at the top and a plate at the bottom. A glass window exists in the middle of the cover plate to allow a look onto the chip.
To lead the tubings to the syringe pumps a hole is designed in the middle of the bottom plate. Top and bottom plate are screwed together to ensure sealing of the channels on the chip.

4.6.2 Measurement results

For characterization of the three different waveguide shifter designs two basically different types of measurements were performed:

- At first, the hydrodynamical shifting of the core stream was investigated. Therefore, no light source was needed. Into the core inlet a blue-colored DI water was pumped and through all the other inlets normal DI water was brought in.
- Secondly, the working functionality was observed. Therefore, the already described light source was used. The light was guided through a glass fiber with a diameter of 80μm. The core liquid was chosen to be a solution of 5mol $CaCl_2$ per liter DI water. The index of refraction at 21°C is measured to be 1.446 [LWL$^+$08]. The cladding and pushing inlets were filled with DI water (index of refraction at 21°C: 1.333 [LWL$^+$08]).
  The pool for visualization of the out coming light was filled with an aqueous Rhodamine B solution.

4.6.2.1 Design one - Simplest realization

Hydrodynamical shifting:

Figure 4.19 shows images of shifting the waveguide towards the middle (4.19(a)), downwards (4.19(b)) and upwards (4.19(c)) in the channel.

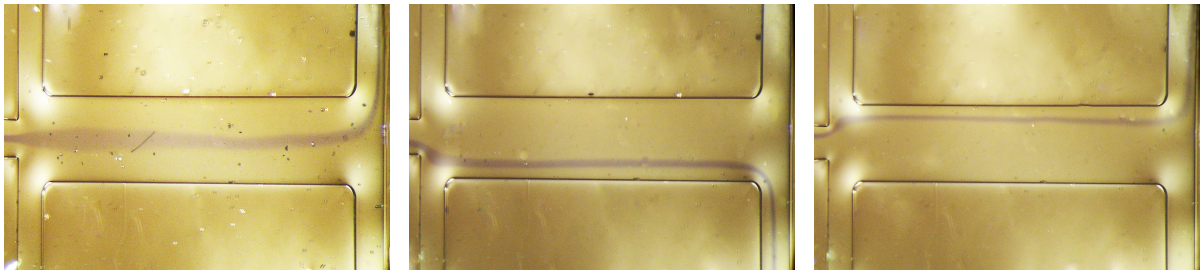

(a) (b) (c)

Figure 4.19: Hydrodynamical shifting of the core fluid visualized by pumping blue colored DI water through the core inlet

To obtain the images shown in figure 4.19 the following inlet velocities have been chosen:

Hydrodynamical shifting - Design one			
Type of velocity	To the middle 4.19(a)	Downwards 4.19(b)	Upwards 4.19(c)
core velocity	2 μL/min	2 μL/min	2 μL/min
upper cladding velocity	8 μL/min	13 μL/min	6 μL/min
lower cladding velocity	8 μL/min	5 μL/min	12 μL/min
upper pushing velocity	8 μL/min	13 μL/min	6 μL/min
lower pushing velocity	8 μL/min	5 μL/min	13 μL/min

Table 4.4: Inlet velocities for hydrodynamical shifting of the core stream as shown in figure 4.19

The images show that shifting upwards and downwards is working well. The results are similar to simulations.
One problem occurs when shifting the core stream towards the middle of the channel. In the simulation it was shown that the core should be split at the end of the chip and guided equally to both outlets. In reality always one outlet is used for the outflow of the entire core liquid.

Working functionality:

Figure 4.20 shows images of the working functionality of this waveguide shifter design. To emphasize the light emitted due to fluorescence a filter was placed over the measurement setup to eliminate green laser light. This results in a mostly black picture on which the emitted light due to fluorescence is perfectly visible.

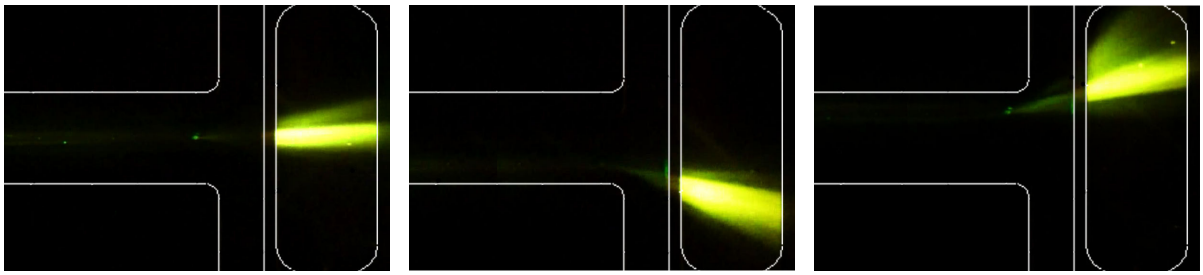

(a) (b) (c)

Figure 4.20: Real working functionality of the device: The $CaCl_2$ core guides the light and is shifted due to different inlet velocities. The exiting light is visualized in the Rhodamine pool

To obtain the images shown in figure 4.20 the following inlet velocities have been chosen:

Shifting of light - Design one			
Type of velocity	To the middle 4.20(a)	Downwards 4.20(b)	Upwards 4.20(c)
core velocity	1.5 μL/min	1.5 μL/min	1.5 μL/min
upper cladding velocity	20 μL/min	22 μL/min	15 μL/min
lower cladding velocity	20 μL/min	16 μL/min	23 μL/min
upper pushing velocity	20 μL/min	23 μL/min	15 μL/min
lower pushing velocity	20 μL/min	15 μL/min	24 μL/min

Table 4.5: Inlet velocities for shifting light as shown in figure 4.20

The basic principle is working well. On figure 4.20(a) the out coming beam is visualized in the middle of the design, on figure 4.20(b) the beam is moved a bit downwards and on figure 4.20(c) it is moved upwards. Referring to the simulation results the inlet velocities of upper and lower cladding and upper and lower pushing have to be swapped for changing from shifting downwards to shifting upwards. In reality they have to be slightly adapted due to different conditions at the two outlets.
The inlet velocities above depict another interesting fact. The core velocity differs heavily from simulation values. It is explained easily: The simulations were done for proving the hydrodynamical shifting functionality. Therefore, properties of water were used. In the final setup used for waveguide shifting the core was changed to the $CaCl_2$ solution. This solution has a much higher compressibility than water and therefore much lower inlet velocities are sufficient to achieve a similar core width compared to the simulations.

4.6.2.2 Design two - Advanced device

Hydrodynamical shifting:

Figure 4.21 shows images of shifting the waveguide towards the middle (4.21(a)), downwards

(4.21(b)) and upwards (4.21(c)) in the channel. The pictures are similar to these taken of the first design.

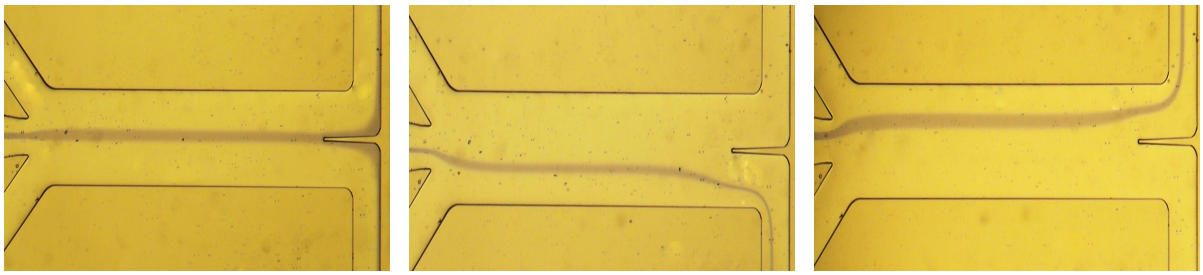

(a) (b) (c)

Figure 4.21: Hydrodynamical shifting of the core fluid visualized by pumping blue colored DI water through the core inlet

To obtain the images shown in figure 4.21 the following inlet velocities have been chosen:

Hydrodynamical shifting - Design two			
Type of velocity	To the middle 4.21(a)	Downwards 4.21(b)	Upwards 4.21(c)
core velocity	2 μL/min	2 μL/min	3 μL/min
upper cladding velocity	7 μL/min	10 μL/min	5 μL/min
lower cladding velocity	7 μL/min	7 μL/min	10 μL/min
upper pushing velocity	7 μL/min	10 μL/min	5 μL/min
lower pushing velocity	7 μL/min	4 μL/min	10 μL/min

Table 4.6: Inlet velocities for hydrodynamical shifting of the core stream as shown in figure 4.21

Hydrodynamical shifting of the waveguide is principally working. By choosing proper inlet velocities the working principle was proved perfectly. Compared to the first design also shifting towards the middle works well. The core is split by the tip and both outlets are used equally.
The tabular with the values of the inlet velocities shows that shifting downwards and upwards is not working equally. The inlet velocities have to be changed slightly from the simulated values. This can be explained with different conditions at both outlets. During measurements it was observed that anytime one outlet is preferred and is used more than the other. Therefore, a change in inlet velocities has to be undertaken to compensate this error.

Working functionality:

Figure 4.22 shows images of the real working functionality of this waveguide shifter design. Again a filter was placed over the measurement setup to eliminate green laser light and emphasize light emitted due to fluorescence.

To obtain the images shown in figure 4.22 the following inlet velocities have been chosen:

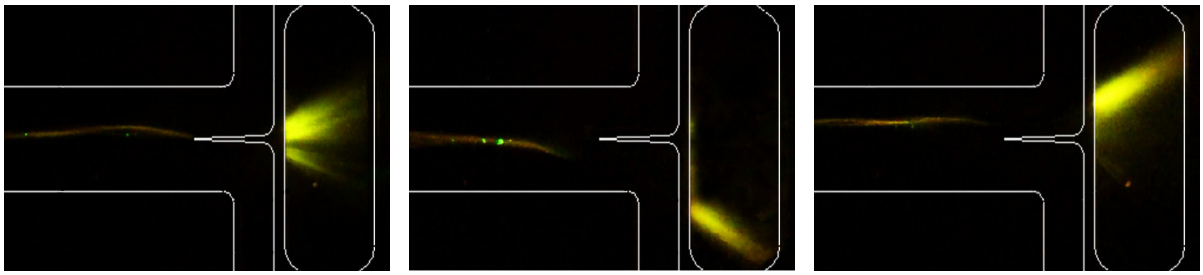

(a) (b) (c)

Figure 4.22: Real working functionality of the device: The $CaCl_2$ core guides the light and is shifted due to different inlet velocities. The exiting light is visualized in the Rhodamine pool

Shifting of light - Design two			
Type of velocity	To the middle 4.22(a)	Downwards 4.22(b)	Upwards 4.22(c)
core velocity	1.5 μL/min	1.5 μL/min	1.5 μL/min
upper cladding velocity	20 μL/min	23 μL/min	17 μL/min
lower cladding velocity	20 μL/min	17 μL/min	23 μL/min
upper pushing velocity	20 μL/min	23 μL/min	16 μL/min
lower pushing velocity	20 μL/min	15 μL/min	24 μL/min

Table 4.7: Inlet velocities for shifting light as shown in figure 4.22

Figure 4.22 depicts the functionality of this design. Especially shifting downwards (4.22(b)) and upwards (4.22(c)) is working well. One problem is visible on figure 4.22(a). The out coming light beam is not focused. Far from it, the light is scattered in many directions. The reason for this phenomenon is the tip placed in the middle of the outlet region. Of advantage for flow stabilization and balancing both outlets, it is of disadvantage for light guiding. Light which hits the tip is not guided anymore within the core but scattered in almost every direction. This fact makes such tips counterproductive for the use in waveguide shifters.
Again, as already figured out by using the first design, the core velocity has to be chosen much smaller compared to simulations.

4.6.2.3 Design three - Additional features integrated

Hydrodynamical shifting:

Figure 4.23 shows images of shifting the waveguide towards the middle (4.23(a)), downwards (4.23(b)) and upwards (4.23(c)) in the channel.

To obtain the images shown in figure 4.23 the following inlet velocities have been chosen:

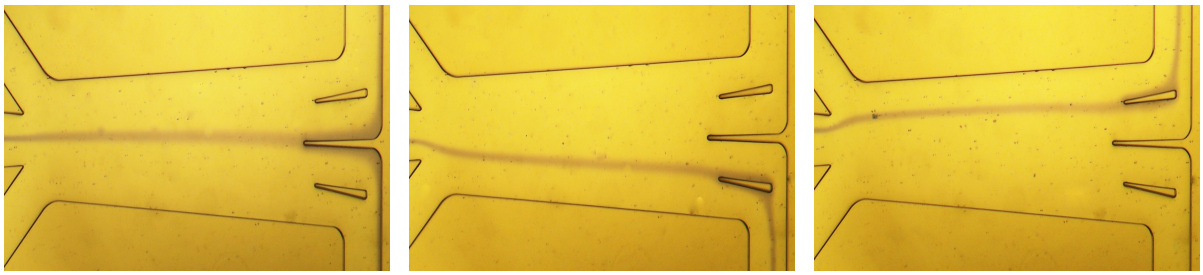

(a) (b) (c)

Figure 4.23: Hydrodynamical shifting of the core fluid visualized by pumping blue colored DI water through the core inlet

Hydrodynamical shifting - Design three			
Type of velocity	To the middle 4.23(a)	Downwards 4.23(b)	Upwards 4.23(c)
core velocity	2 μL/min	2 μL/min	2 μL/min
upper cladding velocity	10 μL/min	13 μL/min	6 μL/min
lower cladding velocity	10 μL/min	8 μL/min	13 μL/min
upper pushing velocity	10 μL/min	13 μL/min	6 μL/min
lower pushing velocity	10 μL/min	5 μL/min	15 μL/min

Table 4.8: Inlet velocities for hydrodynamical shifting of the core stream as shown in figure 4.23

Also in the last design, hydrodynamical shifting of the core stream is working well. The middle tip is of advantage for splitting the core. The side tips seem to fulfill the expectation of fixing the core on these certain positions. Furthermore, the core is turned towards the nearest outlet sharply which should result in good coupling out of light.

Working functionality:

During measurements with the third design several facts have been figured out already. It was known that velocities for the core inlet have to be chosen much smaller than simulated. Furthermore, it was expected that similar to design two the tips placed at the outlet region will be of disadvantage for waveguide shifting applications.
One difference which has not been investigated at this time was the enlargement of the shifting channel.

Shifting the light towards the middle (4.24(a)), downwards (4.24(b)) and upwards (4.24(c)) is shown on figure 4.24.

To obtain the images shown in figure 4.24 the following inlet velocities have been chosen:

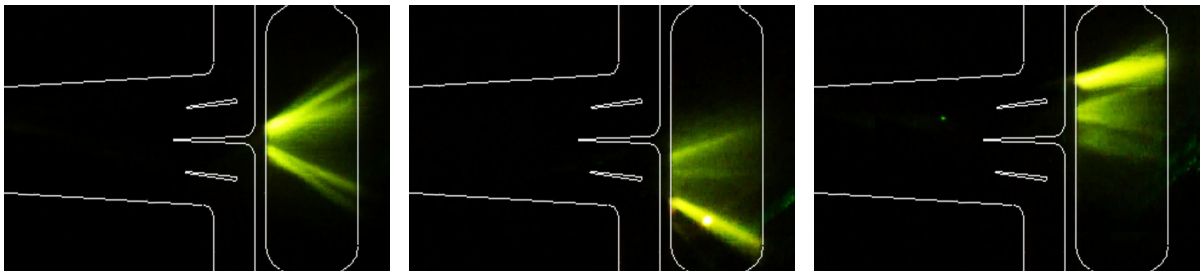

(a) (b) (c)

Figure 4.24: Real working functionality of the device: The $CaCl_2$ core guides the light and is shifted due to different inlet velocities. The exiting light is visualized in the Rhodamine pool

Shifting of light - Design three			
Type of velocity	To the middle 4.24(a)	Downwards 4.24(b)	Upwards 4.24(c)
core velocity	1.5 μL/min	1.5 μL/min	1.5 μL/min
upper cladding velocity	20 μL/min	24 μL/min	16 μL/min
lower cladding velocity	20 μL/min	17 μL/min	24 μL/min
upper pushing velocity	20 μL/min	25 μL/min	15 μL/min
lower pushing velocity	20 μL/min	16 μL/min	24 μL/min

Table 4.9: Inlet velocities for shifting light as shown in figure 4.24

As expected before starting the measurement the tips are of big disadvantage for the use as waveguide shifter. The light is scattered by these tips and radiates in almost any direction. This destroys all the light confinement realized by the difference in the indices of refraction of cladding and core fluid.

The enlargement of the shifting channel was detected to be an improvement. The ability to steer the core upwards and downwards in the channel was increased. This results in higher shifting functionality of the device which would enable the device to use even more than three distinct outlet positions for the light.

4.7 Simulation versus Measurement

In the measurement result section simulation and measurement were compared already shortly. The hydrodynamical shifting works similar in both simulation and reality.
Furthermore, the position of the core in the channel was measured and compared with simulation results. The following sections show diagrams which depict this comparison.

4.7.1 Design one - Simplest realization

At first design one was investigated. Therefore, in both simulation and measurement all inlet velocities were kept the same just one was altered and the position of the core in the channel was measured. For the following diagrams the core velocity was chosen to be 0.8μL/min and all the others, except the altered one, were 20μL/min.
At the ordinate the position of the core in the channel is depicted. It starts at 0μm and goes up to the full width of the channel which is 714μm. At the abscissa the altered velocity is plotted from 5μL/min up to 30μL/min.

Figure 4.25(a) depicts the results for changing the upper cladding inlet velocity and figure 4.25(b) for changing the upper pushing inlet velocity. The simulated data is drawn in blue and the measured in red.
It can be seen that both upper pushing and upper cladding have a similar effect on the core position in the channel. There are two different kinds of errors appearing on these diagrams. The first one is an offset error. If the altered velocity is 20μL/min, which is then the same as all the other inlet velocities, the core should be positioned exactly in the middle at 357μm. In reality that is not the case. Due to the preference for one of the two outlets, in this case the outlet close to the 0μm-position, the core tends more towards this channel side. The offset error is measured and averaged to 50μm.
The other error is a pitch error. It can be said that a change has a bigger influence in reality than in simulation. One reason could be friction on the channel walls. If just little liquid is between core an channel wall this liquid experiences a higher friction force and the effective velocity is reduced. If more liquid is between core and channel wall this friction is of less importance. This would result in a lower effective velocity close to the channel which would explain the pitch error.

The same measurements were performed with lower cladding and pushing inlets as well. Since these comparisons led to the same results the diagrams are not shown in here.

4.7.2 Design two - Advanced device

Similar to the comparison done with design one also for these series of measurements the core velocity was set to 0.8μL/min and all inlet velocities except the altered one were set constantly to 20μL/min.
On the abscissa the velocity is increased from 5μL/min up to 30μL/min. Since design two has a channel width of 814μm the ordinate starts at 0μm and goes up to 814μm.

Figure 4.26(a) shows simulation and measurement data of changing the upper cladding inlet velocity. Figure 4.26(b) shows the same for the upper pushing velocity. Again these to inlets have almost the same influence on the core position.
As before, two errors occur, the offset error, explained due to the preference for one of the two outlets, and the pitch error. Since design two has a tip mounted in the middle of the outlet region the offset error should be decreased. For this design the offset error is determined to be approximately 45μm. Compared to design one without tip this is an improvement of 5μm.
Since the shifting channel of design one and design two are similar also the pitch error can be explained identically. The channel width in case of design two is increased to 814μm but this fact

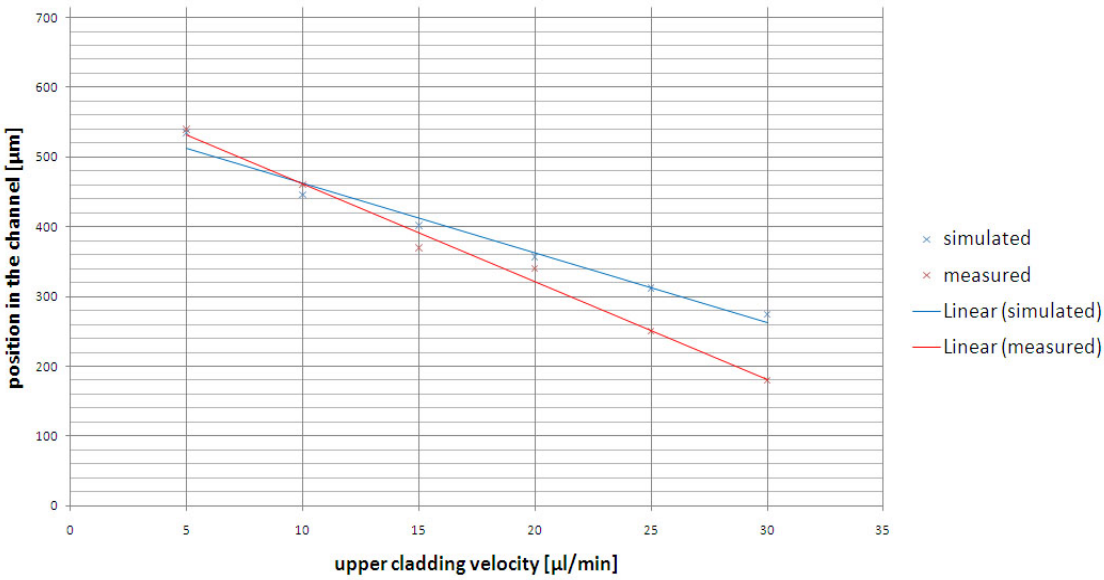

(a) The inlet velocity for the upper cladding has been changed while keeping all the others at a constant value

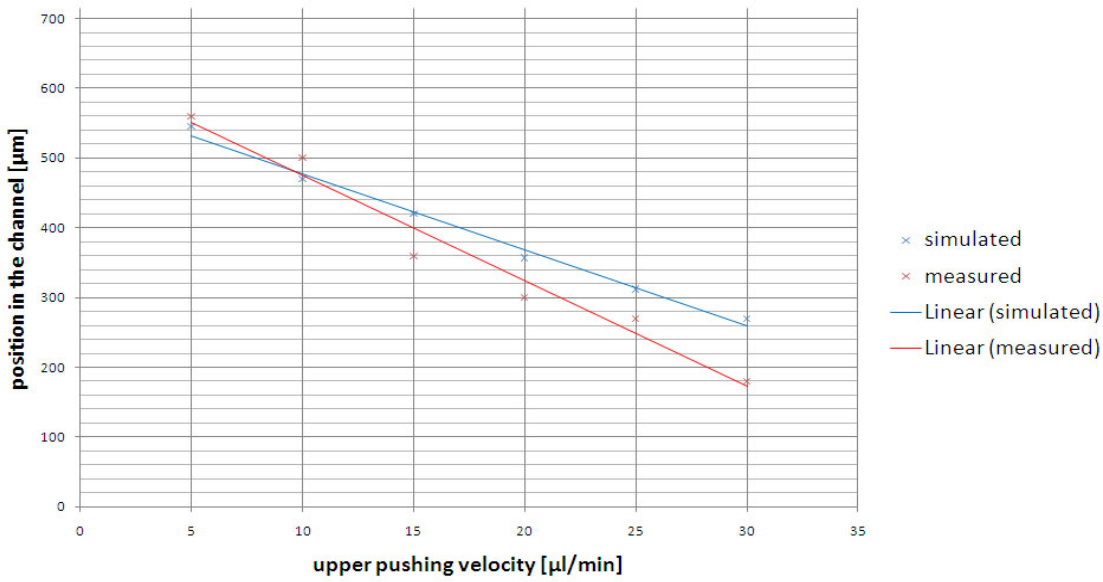

(b) The inlet velocity for the upper pushing has been changed while keeping all the others at a constant value

Figure 4.25: Simulation vs measurement for design one

has no effect on this phenomenon. The friction on the channel wall stays the same and close to the channel walls the effective velocity is smaller than it is set to. In the middle of the channel the influence is a minimum and increases again towards the other channel wall.

Diagrams for altering the lower cladding and pushing velocity were drawn as well. Since the effects are respectively the same as for the upper cladding and pushing these diagrams are not

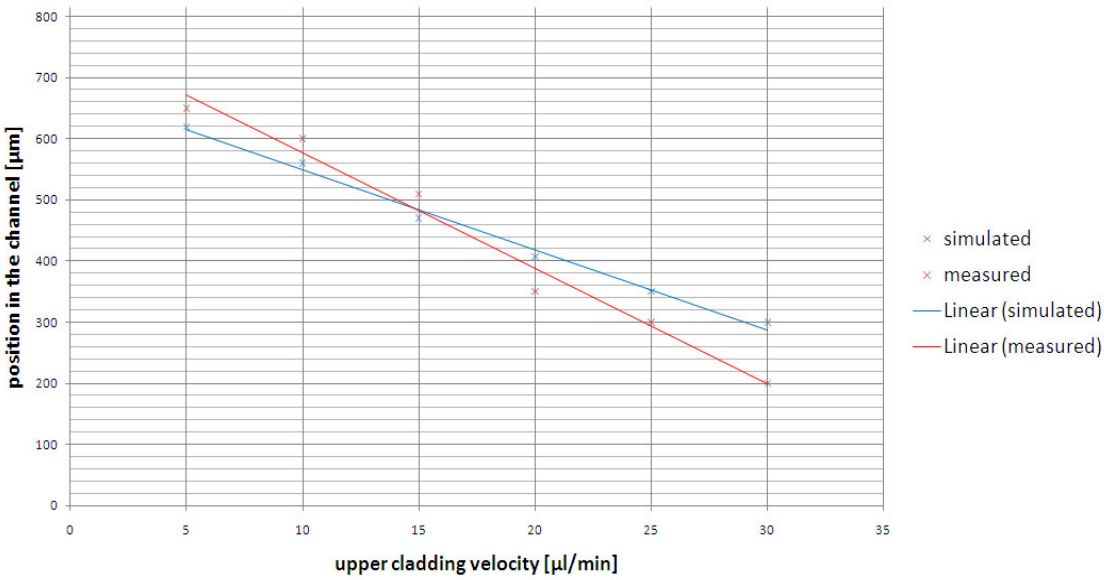

(a) The inlet velocity of the upper cladding has been changed while keeping all the others at a constant value

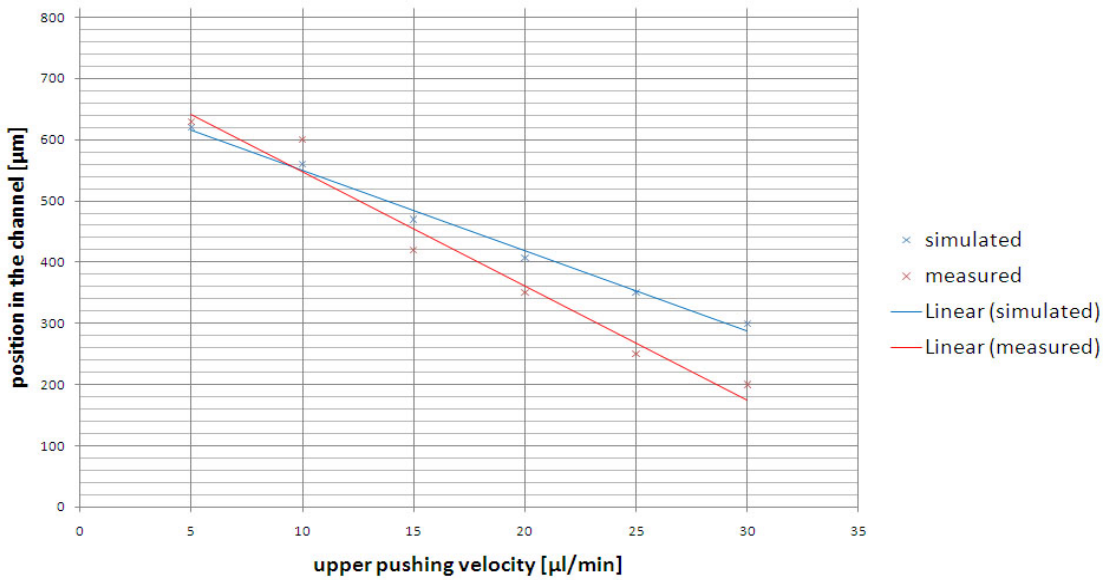

(b) The inlet velocity of the upper pushing has been changed while keeping all the others at a constant value

Figure 4.26: Simulation vs measurement for design two

placed in this work.

4.7.3 Design three - Additional features integrated

Finally, the core position in the third design was analyzed. At the abscissa of the diagrams the velocity is changed from 5μL/min up to 30μL/min. The ordinate starts at 0μm and goes up to 1080μm since the width of the shifting channel close to the outlet is exactly this value.
The core velocity was set to 0.8μL/min and all the other inlet velocities except the altered one were set to 20μL/min.

Figure 4.27(a) and figure 4.27(b) depict the diagrams for changing the upper- cladding and pushing velocities respectively.
Two interesting improvements compared to the other designs are visible. The offset error is still there but it is further improved compared to the other designs. It is reduced to 40μm. This is an improvement of another 5μm. The three tips placed at the outlet region are supposed to be the reason for this improvement. They force the liquid to be split and guided to both outlets equally. Secondly and much more of interest the pitch error is almost perfectly eliminated. This improvement can be explained due to the sloped channel walls of the shifting area. The enlargement of the channel results in less friction force the liquid is exposed to. Therefore, the velocities close to both channel walls are not dramatically reduced and the obtained results are similar to the simulated ones.

Exactly the same conclusions were observed while investigating in altering the lower cladding and pushing inlet velocities. Diagrams of these measurements are not shown in here.

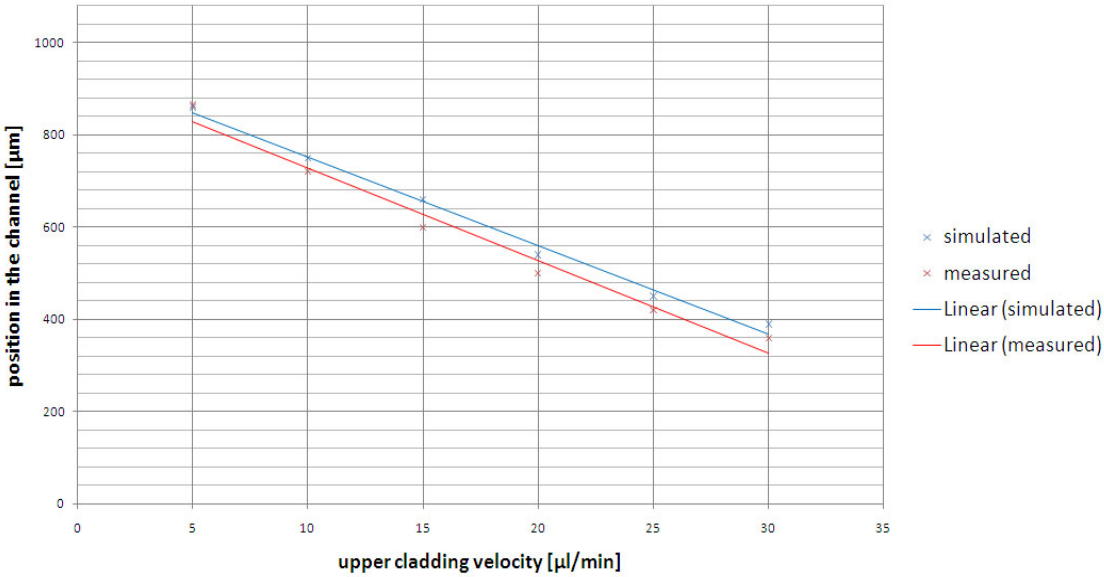

(a) The inlet velocity of the upper cladding has been changed while keeping all the others at a constant value

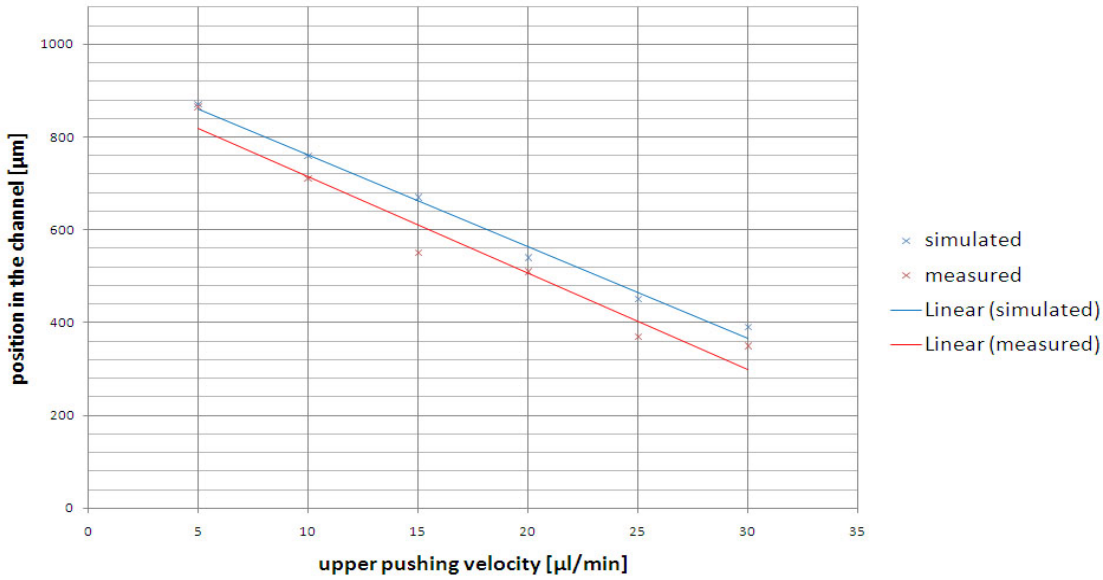

(b) The inlet velocity of the upper pushing has been changed while keeping all the others at a constant value

Figure 4.27: Simulation vs measurement for design three

4.8 Bottom line

Before starting the next section a short summary should be done. In the previous section several useful information could be obtained:

- The chosen 5mol $CaCl_2$ per liter DI water solution for the core medium and DI water for the surroundings are well usable for guiding of light. Losses are observed but they are in an acceptable range.
- Hydrodynamical shifting or, more in general, manipulation of liquids works similarly than simulated. The liquids follow altering of velocities shortly delayed one-to-one.
- Due to the higher compressibility of the chosen $CaCl_2$ solution the velocity for the core inlet has to be small compared to inlets where DI water is pumped in.
- Increasing width of channels towards the outlet is of advantage for gas-bubble-free measurement setups. In this case gas-bubbles are more likely flushed out from the channels.
- Tips in the outlet region for splitting the liquid would be useful for flow stabilization, but since they scatter light they should not be used for light guiding applications.
- Designs with more than one outlet will always result in unbalanced use of these outlets. Therefore, it should be tried to use just one outlet for one chip.

5 Fluorescence Sensor

In this part a chip for a different optofluidic application is presented. One common attribute is L^2-waveguide. Also this application is placed in the field of these special waveguides.

Especially in medical tasks the interest in fluorescence based measurements is enormous. Several analysis methods are based on the principle of fluorescence. The theory behind this phenomenon is described in the first part of this work.
Such an immense demand for fluorescence based measurements ask for investigations in several fields of research. Since micro- (or even nano-) technology has the big advantage of requiring just little amount of test volume and saving of time, research is done especially in this field.

In the next sections an L^2-waveguide based micro-sensor for fluorescence analysis will be presented.

5.1 Concept and basic description

Fluorescence can be used to analyze particles which are fluorescent by itself or particles which are treated and labeled with fluorescent beats. For both possibilities you need a light source to excite fluorescence.
In the case of microfluidic systems a setup for fluorescence detection can be built up as shown in figure 5.1. This setup was used in previous works already [PBKP08].

It consists out of a light source (OLED - organic light emitting diode) on the bottom, the microfluidic chip in the middle sandwiched between to cross aligned polarizers and a detector (OPD - organic photo diode) on top. Polarizers are used to finally detect just light emitted due to fluorescence and not coming directly from the light source.
For this setup the light emitted from the OLED is used to excite fluorescent media placed in the microfluidic chip. The detector on top detects just light emitted due to fluorescence since all the other light is filter by using this arrangement of the two cross aligned polarizers.

In this work a different setup was chosen. At first the polarizers were eliminated since the applied light source has a certain wavelength and can be filtered by using proper light filters. Secondly, the light is coupled in not from the bottom but from the side of the chip.
To increase the possible area of sensing the light source was designed to be light arising from the evanescent field of an L^2-waveguide.

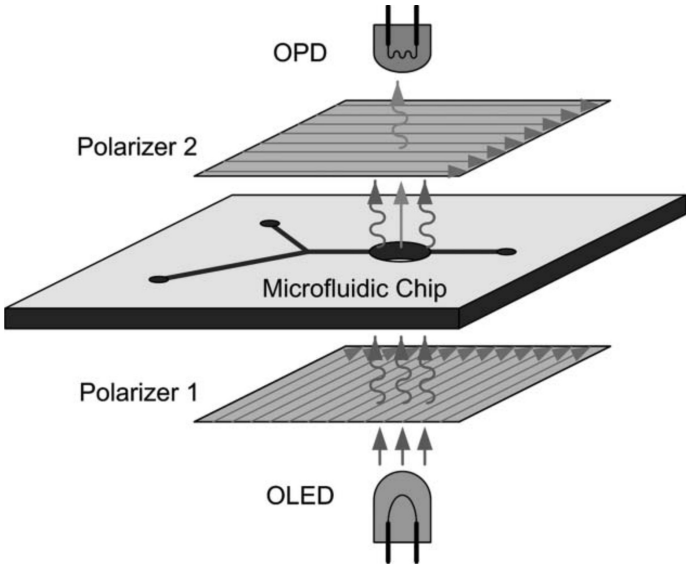

Figure 5.1: Schematic of a possible arrangement to analyze fluorescence on-chip [PBKP08]

Figure 5.2 shows a schematic of the final design-idea of the developed fluorescence sensor.

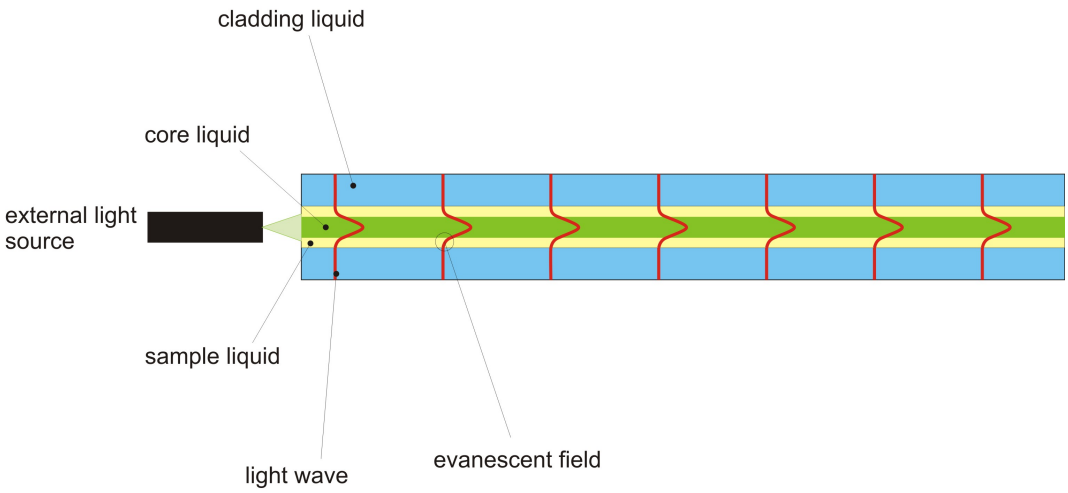

Figure 5.2: Schematic of the final working functionality

The principle working function is as follows:

- Light is coupled into the core of an L^2-waveguide using an external light source.
- The core is sandwiched between two layers filled with the sample fluid.
- Core and sample fluid are sandwiched in between cladding liquid.
- The light is guided mostly inside the core, but, as existing in every waveguide, a small amount of light, the evanescent field, exits the core.

- The evanescent field is used to excite fluorescent media which are inside the sample fluid. This media could be fluorescent liquids or fluorescent particles dispersed in non-fluorescent fluids.
- The emitted light due to fluorescence is detected by using a digital CMOS camera.

The principle of L^2-waveguides was discussed in chapter 4. For these waveguides liquids are used for core and cladding. The difference in the indices of refraction of these two liquids has to be sufficient enough to provide light guiding.
The schematic of the working functionality (5.2) shows that the final device has to contain five inlets. Due to these five inlets, one core-, two sample- and two cladding-inlets, it is even possible to define certain distinct widths for the sample streams. By choosing different inlet velocities different analyzing situations are occurring. Figure 5.3 depicts this functionality.

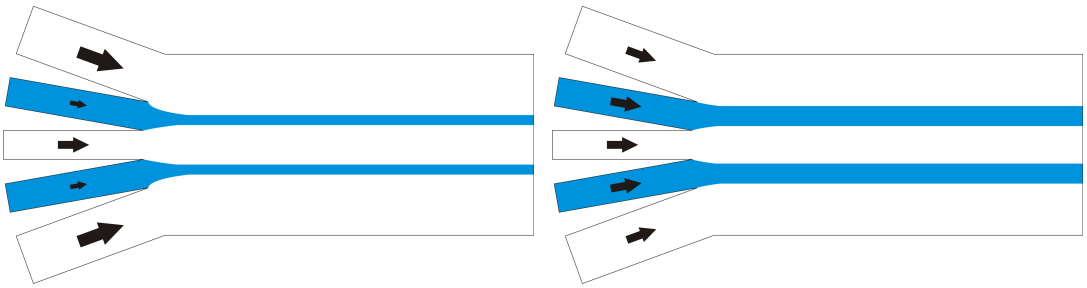

(a) (b)

Figure 5.3: Functionality of defining different sample stream widths

The two blue lines on these figures should depict the sample streams. The arrows on the pictures are drawn proportionally to the inlet velocities. A bigger arrow means higher inlet velocity and vice versa.

By setting the sample velocity to a smaller value and in the same time increasing the cladding velocity (5.3(a)) the width of the sample can be reduced to desired dimensions. Increasing the sample velocity (5.3(b)) results in broader sample streams.

5.2 Developed design

For this chip idea two development steps have been done. At first one design was developed, fabricated and characterized. This "previous design" is treated in the following sections. After analyzing the results, two optimized designs were fabricated. They differ in a few details which will be explained at the end of this chapter.

The idea for the first design is based on a previous work [LWL+08]. In there they provide a design with just three inlets. One for the core and two for the cladding media which, in this setup, is used at the same time as sample liquid.
The big difference and in the end the big improvement compared to this work are two additional inlets for the sample fluid. This provides the possibility of defining different sample stream widths

which was already described above. Furthermore, it can ensure that the sample fluid is brought in tight contact to the core stream. Since the evanescent field exits the core just a little, tight contact to the core is an important factor for fluorescence sensing.
Figure 5.4 shows the COMSOL drawing of this "previous design".

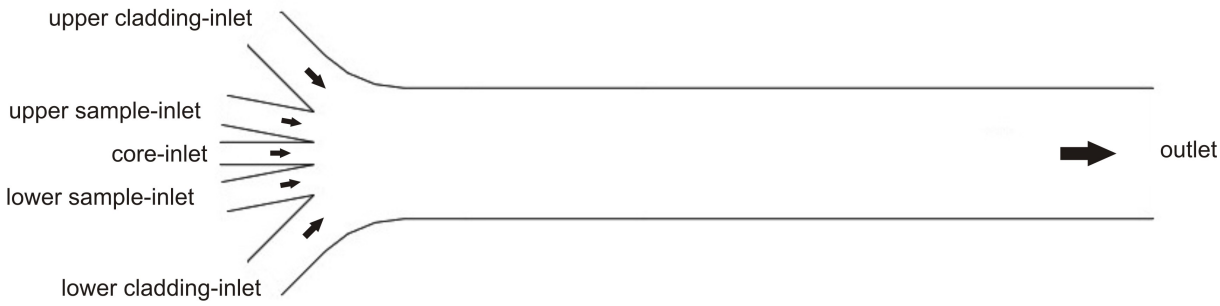

Figure 5.4: COMSOL drawing of the "previous design"

The width of the channel in the middle is 350μm. For more dimensions check the Bricscad drawing which is included later on (5.9).

5.3 Simulation of the developed design using COMSOL

The estimation of the final functionality of the design idea is essential. Therefore, simulations were conducted investigating the design to get a feeling for the working performance of the hydrodynamical manipulation of the sample stream.

5.3.1 Simulation software COMSOL Multiphysics

A short explanation of this simulation software COMSOL Multiphysics was given in a previous section. Please check the simulation part of chapter 4 to get information about.

5.3.2 Simulation results

In order to ensure the ability of the first design to change the width of the sample streams by choosing different inlet velocities simulations were done for two settings of velocities.

Figure 5.5 shows the simulation results for following settings of the inlet velocities:

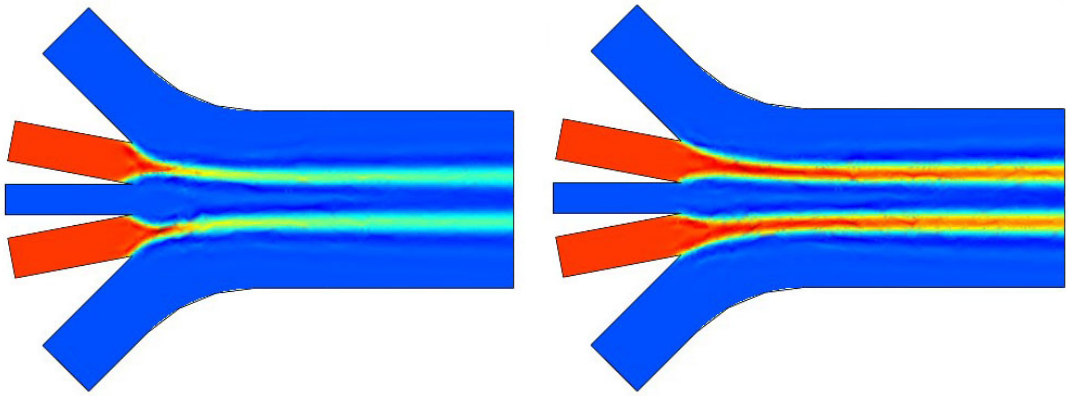

(a) (b)

Figure 5.5: Simulation results for different widths of the sample streams

Simulation of hydrodynamical focusing		
Type of velocity	Small sample width 5.5(a)	Wide sample width 5.5(b)
core velocity	10 μL/min	10 μL/min
upper sample velocity	1 μL/min	3 μL/min
lower sample velocity	1 μL/min	3 μL/min
upper cladding velocity	8 μL/min	8 μL/min
lower cladding velocity	8 μL/min	8 μL/min

Table 5.1: Inlet velocities for simulations of hydrodynamical focusing as shown in figure 5.5

On the figures core and cladding fluid are colored blue and the sample streams are colored red to obtain good contrast. In the contact region diffusion of core and cladding liquid is visible.
It was shown that defining different widths for the sample stream is possible by choosing different inlet velocities. This fact is expected to be used for bringing the sample stream in tight contact to the core stream. If a bigger sample width is necessary, it can be achieved by setting the velocities to different values.

5.4 Device considerations

Before finally fabricating the device different details of the chip have to be investigated. Starting from coupling in of light up to the outflow of liquid. These details and more are explained in the next sections.

5.4.1 Optical path

The optical path consists out of the light source, a glass fiber and the fixation of the fiber on the chip.

For the light source similar considerations than in chapter 4 were done. Since Rhodamine B was planned to be used for showing different working performances, the wavelength of the light source has to be in the range of sensibility of Rhodamine B. The spectrum of sensibility was already shown and discussed on figure 4.9. The wavelength of the light source was set to 531nm.
A glass fiber with a cladding diameter of 80μm was used to guide light from the light source to the chip. Therefore, the inlet for the fiber on the chip was broadened at the beginning and narrowed down to a width of 80μm at the end. An SEM image of this inlet on the fabricated design is shown in figure 5.6.

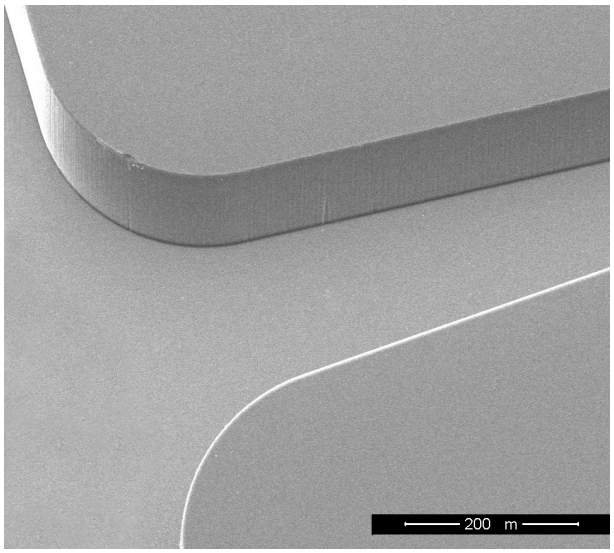

Figure 5.6: SEM image of the glass fiber inlet on the chip

On the left side the glass fiber will be brought in. Because of resolution reasons of the SEM the right side was cut but it can be imagined to be narrowed down to a width of 80 μm. Directly after this part the core inlet is placed which can be seen on the Bricscad drawing of this device attached later on.

5.4.2 Positions of in- and outlets

Since the same device holder was used as for the device presented in chapter 4, the in- and outlets on the chip were placed again on these certain 12 positions. A figure of the holder and more information about it can be found in the device considerations section of chapter 4.

5.4.3 Merging of core, sample and cladding

The next important part of the device is the merging region of core, sample and cladding. To provide a smooth connection between core and sample fluid the sample inlets are arranged in a small angle with respect to the core inlet.
The cladding inlets should be placed in a bigger angle to provide good focusing performance for the sample fluid. Choosing the angle to high would result in higher diffusion in this area.

Therefore, an angle of 45° with respect to the core inlet has been chosen.
Figure 5.7 shows an SEM image of the merging region of the final device.

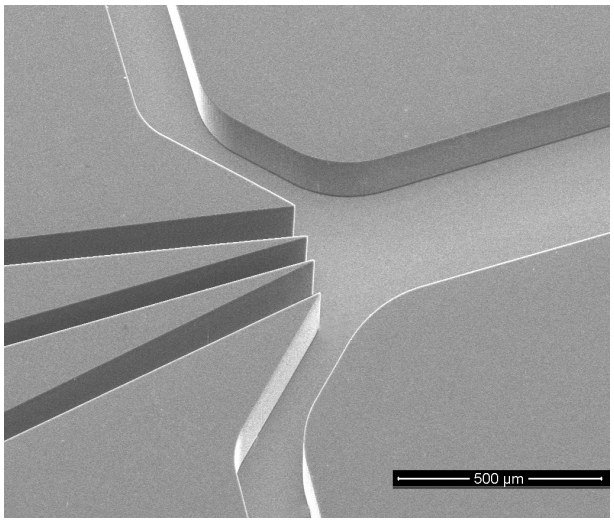

Figure 5.7: SEM image of the merging region of core, sample and cladding

The depth of the channels is 100μm. Generally it was tried to avoid sharp corners to avoid turbulent flow. Therefore, most of the corners are rounded down.

5.4.4 Liquid outflow from the chip

The last detail of this device is the outlet of liquid. It was tried to be designed simple to avoid problems with it. Therefore, just one outlet was placed in the middle of the chip.
Figure 5.8 shows an SEM image of this part of the finally fabricated device.

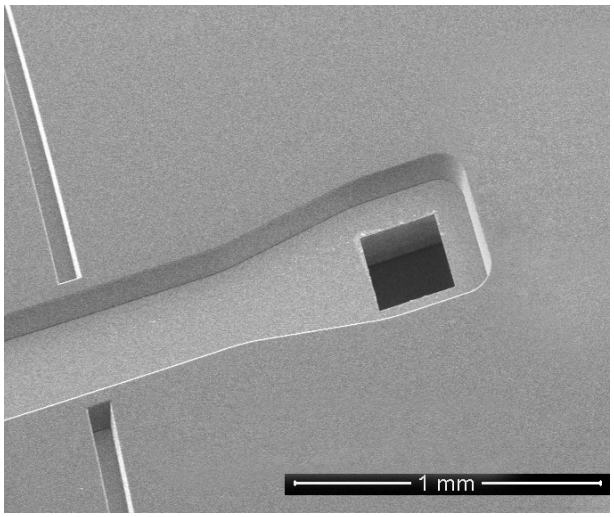

Figure 5.8: SEM image of the outlet region

Between the images showing the merging region (5.7) and the outlet (5.8) a channel with constant width and a length of approximately 2mm can be imagined.

5.5 Layout of the final device

In the first development step one design for the fluorescence sensor was fabricated.
Figure 5.9 shows the Bricscad drawing and figure 5.10 shows a picture of the real device.

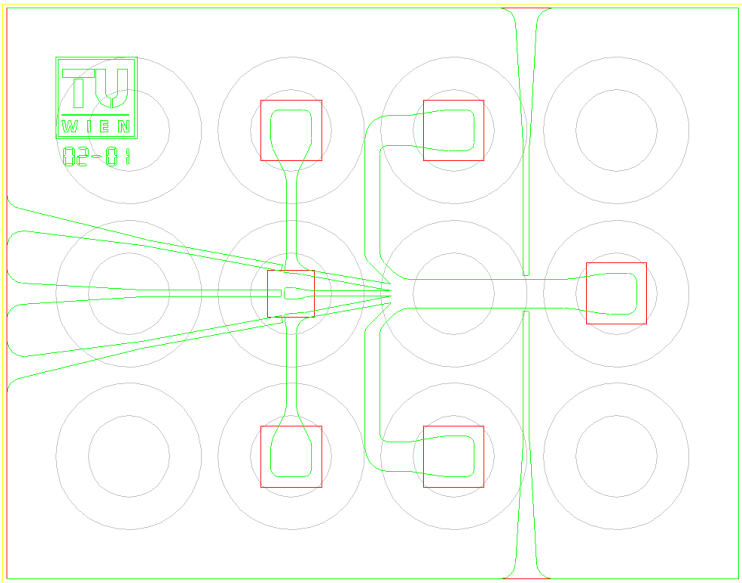

Figure 5.9: Bricscad drawing of the fabricated fluorescence sensor

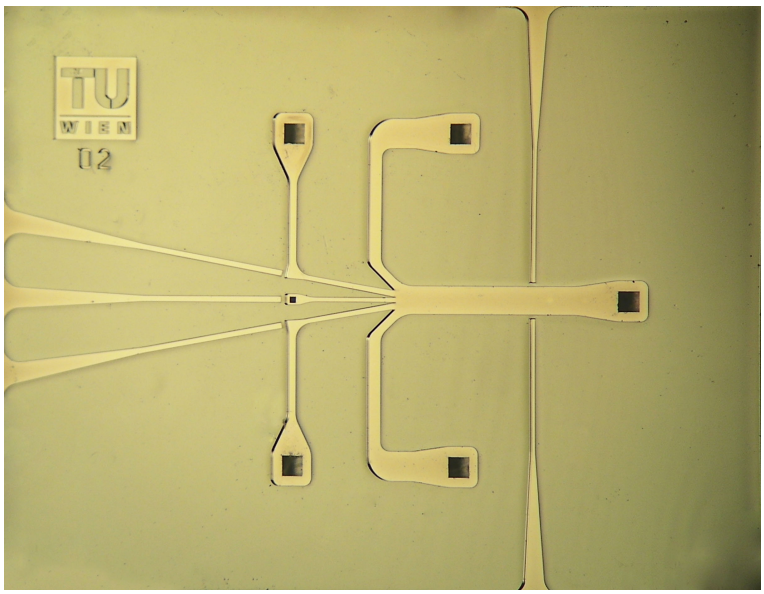

Figure 5.10: Image of the final device

5.6 Measurements

5.6.1 Experimental setup

The same setup used already in chapter 4 was taken again to characterize this device. Just a different laser with higher output power (4mW; 531nm) was used. To avoid repetitions in this work no sketch of the measurement setup is placed at this position. For more details check the measurement section of chapter 4.

5.6.2 Measurement results

For analyzing the working behavior of the device two different measurements were performed. The first one to show the hydrodynamical focusing of the sample stream and the second one to show the real working performance.

Hydrodynamical focusing:

At first the hydrodynamical focusing of the sample fluid was investigated. As simulated before different widths of the sample fluid were expected by choosing different inlet velocities. Figure 5.11 shows pictures of two obtained sample widths. Core and cladding liquid were colored green and the sample liquid was colored red DI water to obtain good contrast.

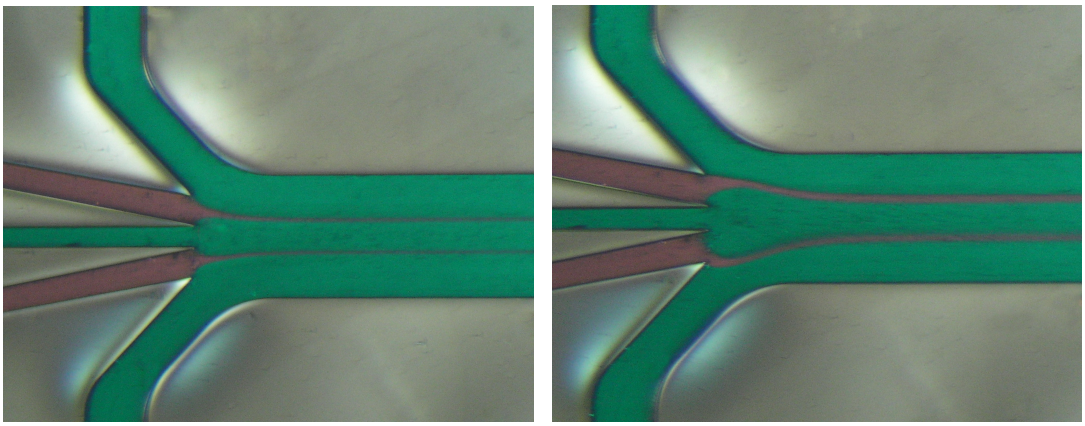

(a) (b)

Figure 5.11: Hydrodynamic focusing of the sample stream visualized by using colored DI water

To obtain picture 5.11(a) and picture 5.11(b) the following inlet velocities have been chosen:

Hydrodynamical focusing		
Type of velocity	Small sample width 5.11(a)	Wide sample width 5.11(b)
core velocity	2 μL/min	2 μL/min
upper sample velocity	1 μL/min	3 μL/min
lower sample velocity	1 μL/min	3 μL/min
upper cladding velocity	10 μL/min	10 μL/min
lower cladding velocity	10 μL/min	10 μL/min

Table 5.2: Inlet velocities for hydrodynamical focusing of the sample streams as shown in figure 5.11

The figures illustrate that hydrodynamical focusing of the sample width is possible by choosing different inlet velocities. Compared to the simulations the core velocity had to be chosen much smaller to obtain similar results than simulated.

Working functionality:

To investigate the working functionality of the device ethanol was used as core medium, an aqueous Rhodamine B solution as sample and normal DI water as cladding fluid. To eliminate light coming directly from the light source an optical filter was placed between setup and microscope. This should ensure that just light due to fluorescence is visible on the finally obtained pictures.
Again it was tried to obtain different sample stream widths by choosing different inlet velocities. Figure 5.12 shows two obtained pictures.

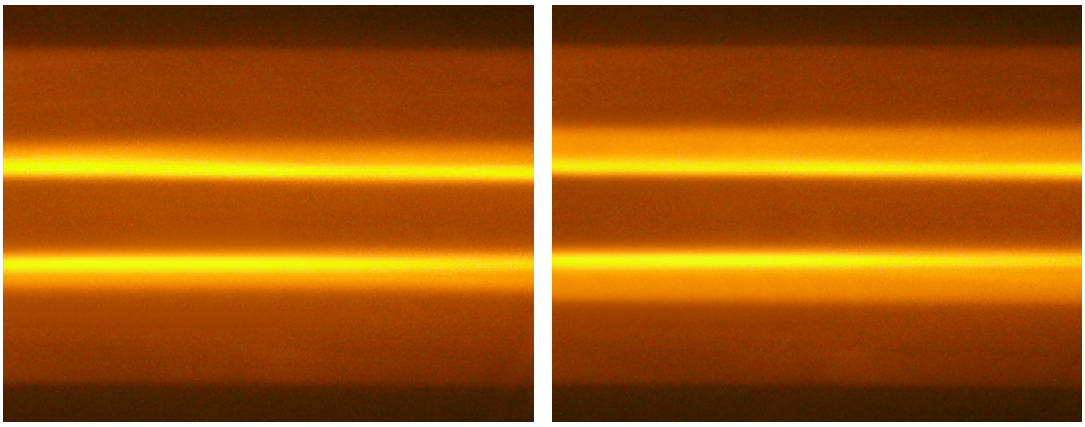

(a) (b)

Figure 5.12: Fluorescence sensor working functionality using an aqueous Rhodamine B solution as sample medium

For figure 5.12 the inlet velocities were chosen as follows:

Fluorescence sensing		
Type of velocity	Small sample width 5.12(a)	Wide sample width 5.12(b)
core velocity	20 μL/min	20 μL/min
upper sample velocity	4 μL/min	10 μL/min
lower sample velocity	4 μL/min	10 μL/min
upper cladding velocity	20 μL/min	20 μL/min
lower cladding velocity	20 μL/min	20 μL/min

Table 5.3: Inlet velocities for fluorescence sensing as shown in figure 5.12

On figure 5.12(a) the sample inlet velocity is set to a smaller value and on figure 5.12(b) it is set to a higher one. On both figures the merging region of the inlets is not shown to highlight the fluorescence sensing part.

In the middle the core stream is visible. An aqueous Rhodamine B solution, which is used as sample medium, is placed on both sides of the core. Due to the fluorescent property of Rhodamine B the sample streams are shining brightly on the figures. On top and bottom the cladding streams can be seen.
Fluorescent light is emitted all over the sample stream width. But close to the core the stream is much brighter than further away. This is due to the evanescent field exiting the core.

Since the evanescent field is not depending on the thickness of the sample streams these bright lines are of same thickness on figure 5.12(a) and figure 5.12(b). Just the width of the sample fluid is different.

Theory versus Reality:

The formula for the penetration depth of the evanescent field into the cladding was given already in the theory part.

$$d_p = \frac{\lambda}{2\pi\sqrt{{n_1}^2 sin^2\Theta - {n_2}^2}} \tag{5.1}$$

λ is given by $531nm$, n_1 is given by the index of refraction of ethanol to 1.3614 and n_2 is the index of refraction of water 1.333. The angle of the incoming light Θ has to be specified more in detail.
Since the angle of the incident light cannot be defined explicitly also d_p is not defined to just one value. The minimum of d_p is obtained if setting Θ to 90°. Than d_p is given by $305.5nm$.
Setting Θ to Θ_{crit} of the L^2-waveguide results in a penetration depth of infinity.

To get a good estimation for the deepest penetration depth, the numerical aperture of the L^2-waveguide is used.

$$NA = \sqrt{n_1^2 - n_2^2} = n_1\sqrt{1 - sin^2\Theta_{crit}} = 0.2766 \tag{5.2}$$

The critical angle for total reflection Θ_{crit} is calculated to slightly less than 78.28°. Taking this

value, which in fact is close to the critical angle, and calculating d_p, the maximum penetration depth for this setup is defined to be $12.4\mu m$.

Out of figure 5.12 the measured penetration depth of the evanescent field is approximately $10\mu m$. This fits quite well to the estimated theoretical maximum penetration depth of the evanescent field of $12.4\mu m$.
The cross-section of the L^2-waveguide shows, that core, sample and cladding fluid are not placed like square bars next to each other. Due to different densities of the used liquids and also due to the arrangement of the pushing inlets the cross-section is distorted. Thus an exact value for the penetration depth of the evanescent field into the sample fluid cannot be determined exactly.

5.6.3 Sample width analysis

For investigation of the sample width following liquids were chosen:
Core and cladding fluids were normal DI water and the sample liquid was colored DI water.

Measurements were performed while keeping core and cladding inlet velocities at a constant level and increasing the velocity of the sample from 0.1μl/min up to 10μl/min. The width of the sample stream was measured and finally printed in a diagram.
Figure 5.13 shows this diagram.

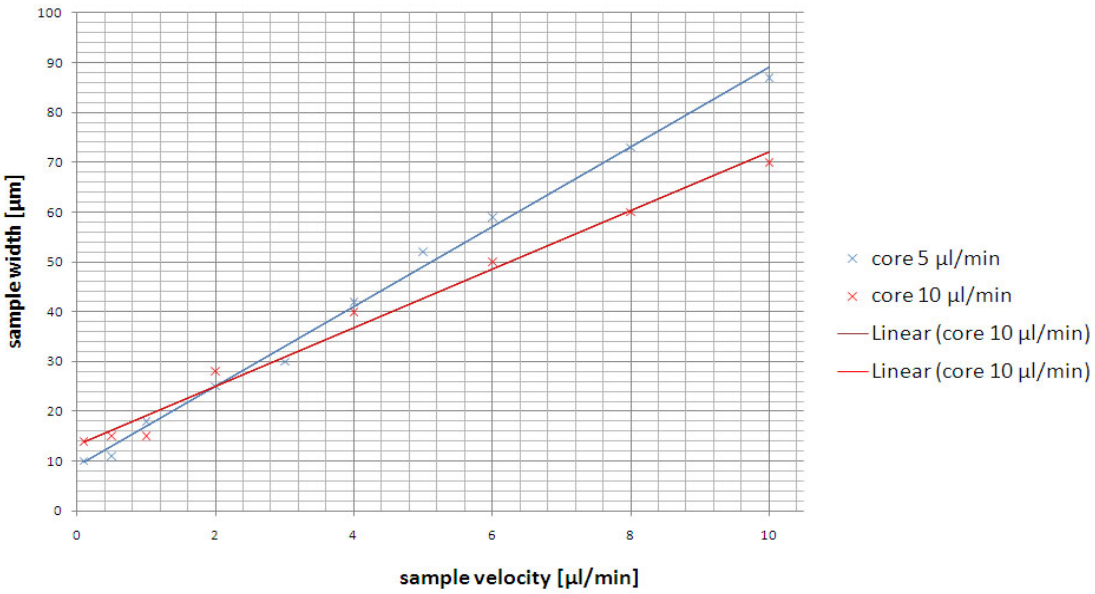

Figure 5.13: Sample width analysis while keeping core and cladding velocities constant and changing the sample velocity

For both lines the cladding velocity was set to 15μl/min. The core velocity was 5μl/min for the blue line and 10μl/min for the red one.
Increasing sample velocity results in increasing width of the sample stream. Furthermore, it can be seen that setting the core velocity to a higher level results in a lower pitch of the curve. That means that higher core velocities result in smaller sample width changes when increasing the sample velocity. The impact of increasing sample velocity is reduced.

A second study was done while keeping core and sample velocities constant and changing the cladding velocity. For the sample velocity 2μl/min has been chosen and the core velocity was 5μl/min and for a second series of measurements 10μl/min.
Figure 5.14 shows the obtained diagram.

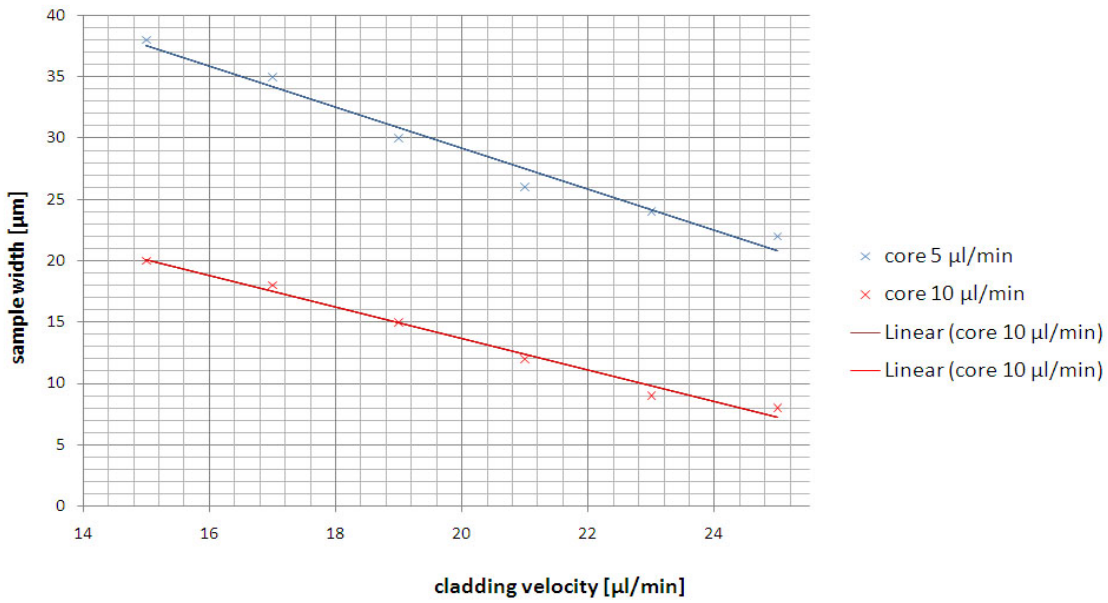

Figure 5.14: Sample width analysis while keeping core and sample velocities constant and changing the cladding velocity

Again the blue line was obtained for a core velocity of 5μl/min and the red one for 10μl/min. Increasing velocity for the cladding fluid results in a smaller sample width. As expected the sample width is generally reduced when using a higher core velocity. Furthermore, the pitch of the line is reduced. As already obtained from the previous measurement this is expressed in lower impact of a change in the cladding velocity when using a higher core velocity.

5.7 First Conclusion

After investigation of the first realized design a small conclusion has to be done:

- The design is working as expected. The arrangement of the inlets was chosen well and also the dimensions of the channel used for the fluorescence analysis was suitable for the application.
- Using just one outlet had advantages in stable flow conditions.
- Losses of light were observed in the glass fiber inlet region of the device.
- It was difficult to adjust the glass fiber to obtain straight light guiding towards the core liquid.

These facts were taken into account and they were tried to be improved and optimized in the next development step.

5.8 Improved devices

As already mentioned at the beginning of this chapter the development of this fluorescence sensor was split into two parts. The first part was discussed in the previous sections.
In the second part the previous design and the obtained conclusions were used to realize an improved design with optimized working functionality.

5.8.1 Design ideas

The biggest problem while using the previously presented design was coupling of light into the core stream. Therefore, this part was tried to be improved on the new designs.

5.8.1.1 Glass fiber inlet

Problems with straight light guiding towards the core liquid were observed while investigating the previously presented design. To eliminate these troubles a special glass fiber inlet was developed. Figure 5.15 shows an SEM image of the glass fiber inlet used for the new designs.

This special inlet consists out of two parts. On the left side the glass fiber inlet is visible. It is broadened on the left and narrowed down to 90μm on the right side. This dimension was chosen to be suitable for an 80μm glass fiber.
Between this glass fiber inlet and the core inlet a waveguide was built up directly on the chip. The core of this waveguide is a bar of SU-8 and a region of air is used as cladding medium. By using this special glass fiber it is ensured that light is guided perfectly straight towards the core inlet.
The beginning of the waveguide can be seen on the right side of figure 5.15 and the end is visible on the left side of figure 5.16.

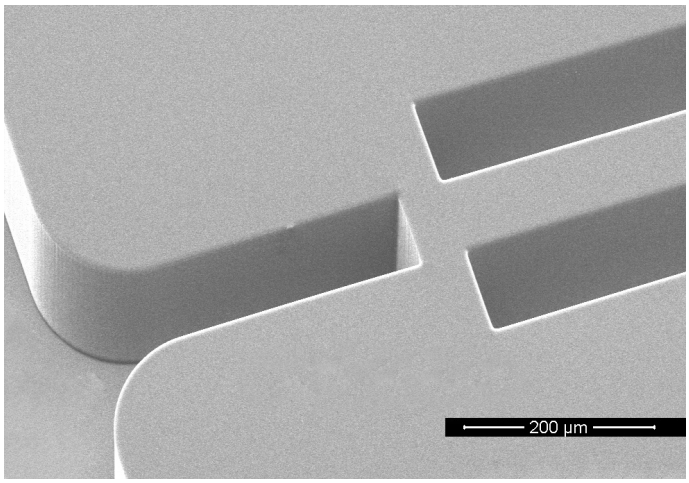

Figure 5.15: SEM image of the glass fiber inlet used for the new designs

5.8.1.2 Merging region of core, sample and cladding inlets

Also the merging of core, sample and cladding inlets was tried to be optimized. In the previously presented design this region was quite far away from the core liquid inlet. This fact is of big disadvantage. In regions where the core is not sandwiched in between the cladding media light is guided with high losses. Therefore, the merging region was placed as close as possible to the core inlet to reduce light losses.
Figure 5.16 shows an SEM image of the optimized merging region used for the new designs.

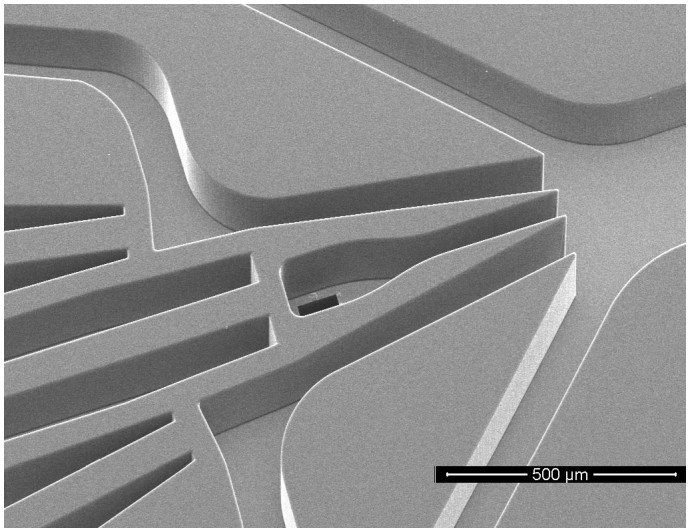

Figure 5.16: SEM image of the merging region of core, sample and cladding used for the new designs

It can be seen that, compared to the previous used merging region, the core fluid is merged with sample and cladding fluid as soon as possible. This should result in lower light losses than detected for the first design.

5.8.1.3 Liquid outlet

To enable the possibility of having a look at the cross section of the L^2-waveguide the outlet region was changed. One solution was designed by using just one and the other by using two outlets.
Figure 5.17 shows both of these realizations.

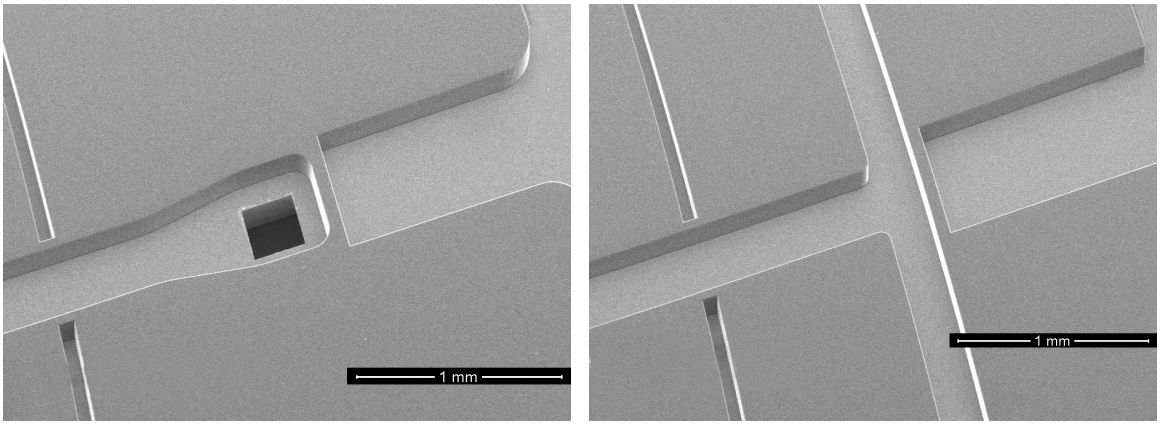

(a) (b)

Figure 5.17: SEM images of the two outlet regions used for the new designs

The realization with just one outlet is shown on figure 5.17(a). A place was prepared right after the outlet. A prism could be placed there which reflects the out coming light from the L^2-waveguide upwards and enables the possibility to have a look on the cross section of the L^2-waveguide.
Figure 5.17(b) depicts the realization with two outlets. Again a place for a prism was prepared. Furthermore, two outlets are used for the outflow of liquid. This should improve the coupling out of light from the L^2-waveguide.

5.8.2 Fabricated devices

Considering the details discussed in the section above two new and improved designs were fabricated.
Figure 5.18 shows the Bricscad drawings of the two devices and figure 5.19 images of the fabricated chips.

- Figure 5.18(a) and figure 5.19(a) show the improved design with just one outlet in the middle of the right part of the chip.
- Figure 5.18(b) and figure 5.19(b) depict the realized device with two outlets, one on the upper side and one the lower side of the right part of the chip.

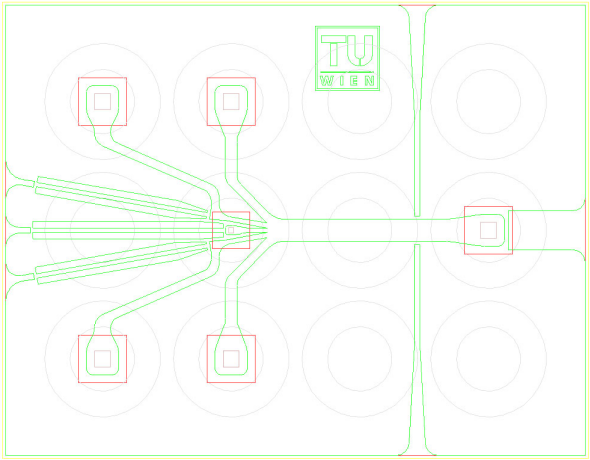

(a)

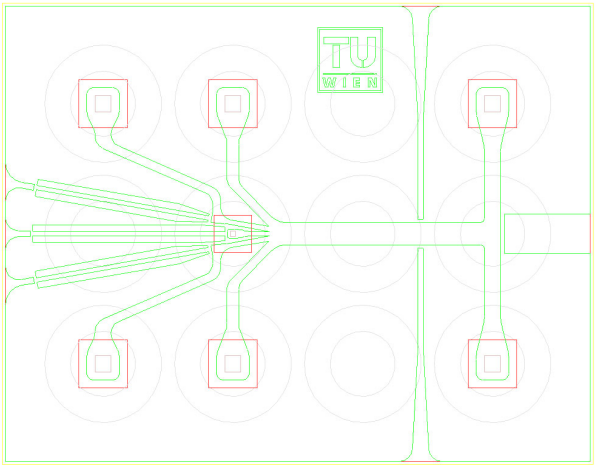

(b)

Figure 5.18: Bricscad drawings of the two optimized designs

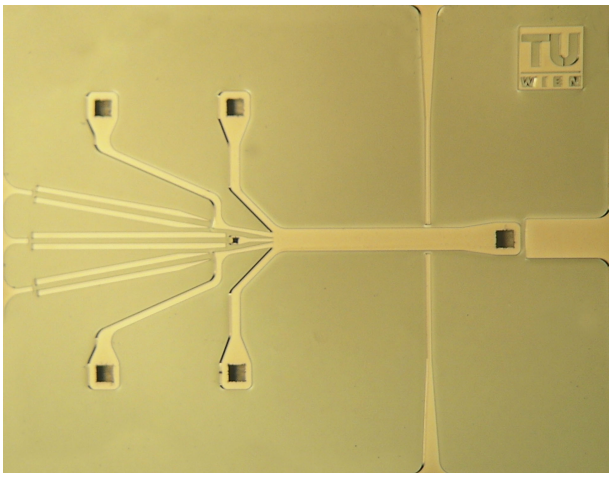

(a)

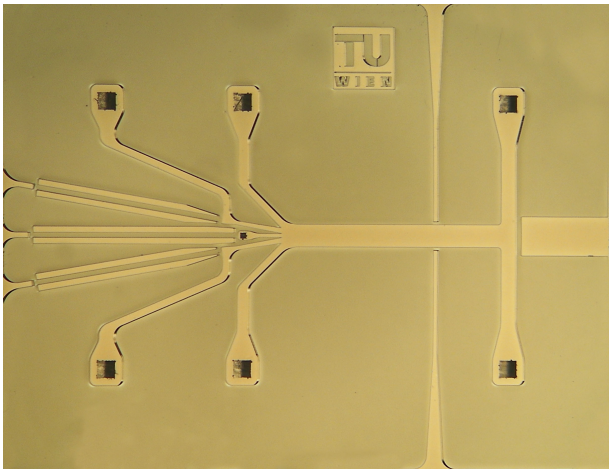

(b)

Figure 5.19: Pictures of the two fabricated optimized devices

5.9 Bottom line

After characterization of the first fabricated design and development of the two new improved designs several different results were obtained:

- The arrangement of the inlets was chosen well. The device had the expected working performance.
- It was possible to focus the sample streams to dimensions less than 10μm. The dimension of the channel where the analysis takes place was suitable.
- Having just one outlet for the device results in more stable flow conditions. This was observed for both realizations.
- Two outlets should be avoided to eliminate unbalances resulting from unequal use of the outlets.
- One of the most critical adjustments is coupling in of light. Therefore, a design containing the glass fiber inlet used for the improved designs is an advantage.
- Losses of light in regions where the core is not sandwiched between cladding medium are enormous. Therefore, this region should be kept as short as possible.

6 Discussion and Conclusion

Two bottom lines were drawn already after both of the developed devices. However, a short summary of all obtained conclusions is placed here at the end of this work. At first, specific facts of each device are listed and secondly an overall conclusion is given.

6.1 Waveguide shifter

The goal of this part was developing a waveguide shifter for an L^2-waveguide. Finally, it should be possible to shift an incoming light beam to different outlet positions.
Simulations were done before starting fabrication of the device and it was proven theoretically that the final device should be able to fulfill upper requirements.

Adapted from previous works [LWL+08] following combination of liquids was used for the setup:

- A 5 mol $CaCl_2$ per liter DI water solution was used as core liquid.
- The cladding medium was chosen to be normal DI water.
- For visualization of the out coming light an aqueous Rhodamine B solution was used.

In later experiments this combination was figured out to be suitable for the application.

Hydrodynamical shifting of the core fluid was tested by using colored DI water as core. The obtained results were similar to simulations and therefore sufficient for the desired behavior of the final device.

By using the $CaCl_2$ solution the real working performance was observed. After adjusting the inlet velocities to a proper level it was possible to steer the out coming light beam upwards and downwards. Different dimensions for the shifting channel were tested and an increasing width was found out to show better working functionality.

Tips in the outlet region are of advantage for flow stabilization. Nevertheless they should not be used in L^2-waveguide applications since they scatter light in almost every direction.
For applications not requiring light guidance they could be useful.

6.2 Fluorescence sensor

Also this device belongs to the field of L^2-waveguides. The goal of the fluorescence sensor was using the evanescent field arising from an L^2-waveguide to excite fluorescence in a sample fluid.

Before starting manufacturing the device simulations were done to prove the hydrodynamical focusing of the sample streams. After analyzing the simulation results the device was supposed to be able to define different sample widths by choosing different inlet velocities.

Following combination of liquids was used for the final setup:

- Ethanol was used as core liquid.
- The cladding medium was chosen to be normal DI water.
- An aqueous Rhodamine B solution was used as sample liquid to visualize fluorescence.

At first the hydrodynamical focusing of the sample streams was investigated. Therefore, differently colored DI water solutions were used for the liquids. Focusing of the sample streams was working well but slightly different to simulations.

Finally, the real working situation was tested and excellent results were obtained. The device fulfilled most of the requirements.

Coupling of light into the core was the biggest challenge. Therefore, optimized devices were developed and finally fabricated.
The glass fiber inlet was changed which ensured straight light guiding towards the core liquid. This adaptations brought advantages and should be applied in later projects.

6.3 Overall conclusions

Specific details about both developed devices were discussed above. Now phenomena observed for both devices are listed:

- Coupling light into the core is a big challenge. To obtain straight light guiding a design with an integrated waveguide on the chip is advantageous.
- To ensure just little losses of light regions of core not sandwiched between cladding fluid have to be made as short as possible.
- Designs with one outlet on the chip provide stable flow conditions. Having more outlets results in unbalances and one outlet will be used more likely than the other one.
- Having a setup without gas-bubbles in the channels is of big importance. Channels enlarging towards the outlet show smaller gas-bubble problems compared to channels having the same width all over the chip.

Concluding it can be said that two well working devices were developed. In a few details they still can be improved to obtain better working performances. Since L^2-waveguides are in the field of interest at the moment an L^2-waveguide shifter could be required in future.
Conducting on-chip analysis results in saving of time and sample medium. Therefore, developing of high-performance fluorescence sensors similar to the developed one will be of interest soon.

6.4 Outlook

The conclusions obtained from the presented devices extended the knowledge of microfluidic systems and will have impacts on further investigations done in these field. Connecting the syringe pumps to a personal computer and hence enable the possibility to control the inlet velocities automatically could further improve the waveguide shifter behavior. The outlet position of the light could be detected and transmitted to a computer frequently. Putting these information into a closed loop and controlling the syringe pumps accordingly could stabilize the flow enormously. The investigated inlet velocities for the fluorescence sensor design were in the range of 4 to 30 μl/min. These velocities are much to high to have visual contact to particles dispersed in the sample medium. Further investigations could be conducted to reduce the velocities to values below 1 μL/min to enable tracking of particles. Furthermore, a second light source with different wavelength could be used to excite fluorescence at two different wavelengths simultaneously and hence increase the analyzing possibilities.

A Mask layouts

A.1 Wafer one

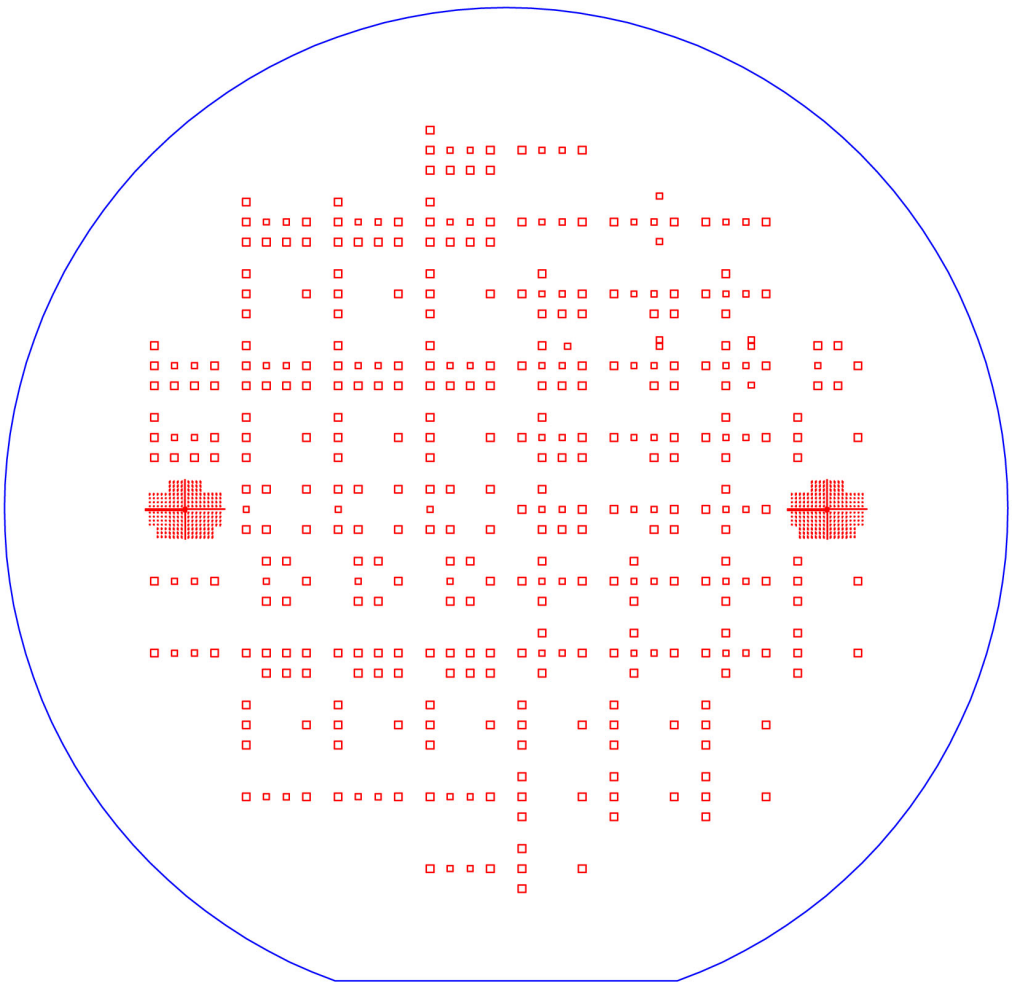

Figure A.1: Mask for etching the holes through the silicon wafer for wafer one

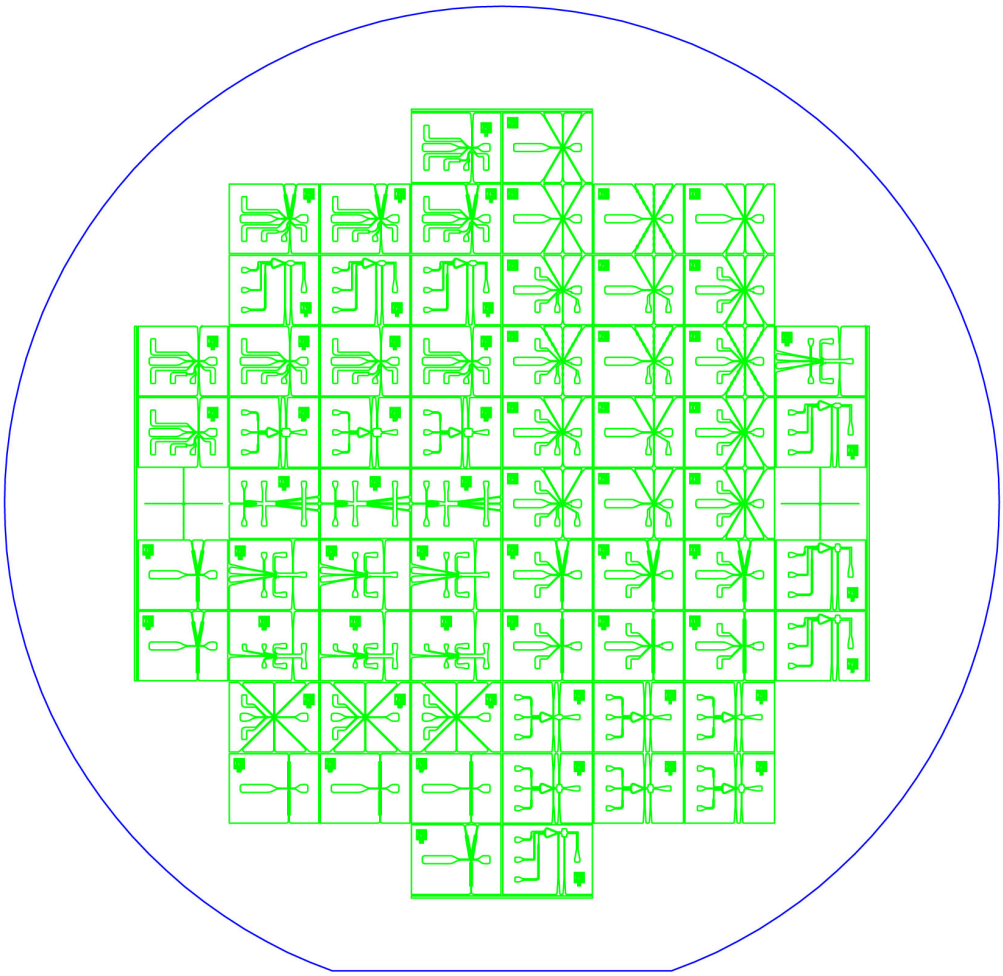

Figure A.2: Mask for structuring the SU-8 layer of wafer one

A.2 Wafer two

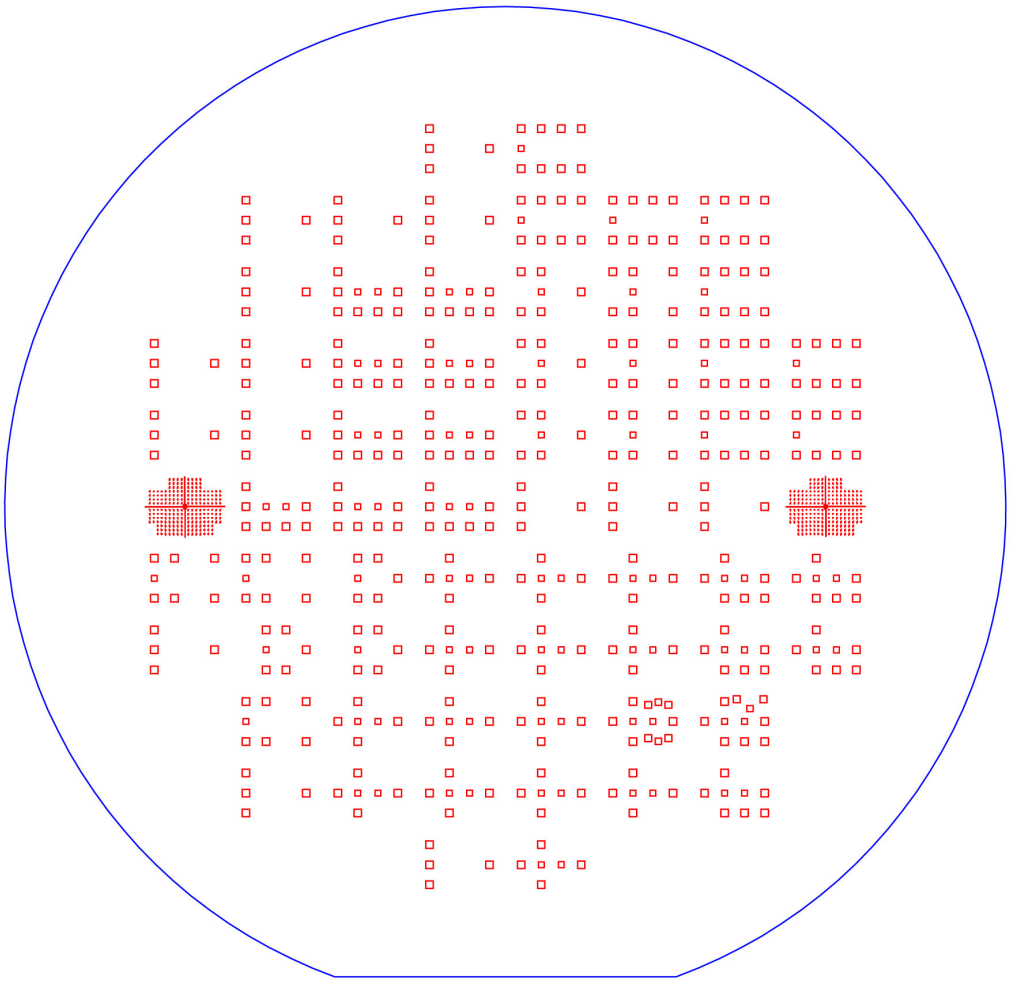

Figure A.3: Mask for etching the holes through the silicon wafer for wafer two

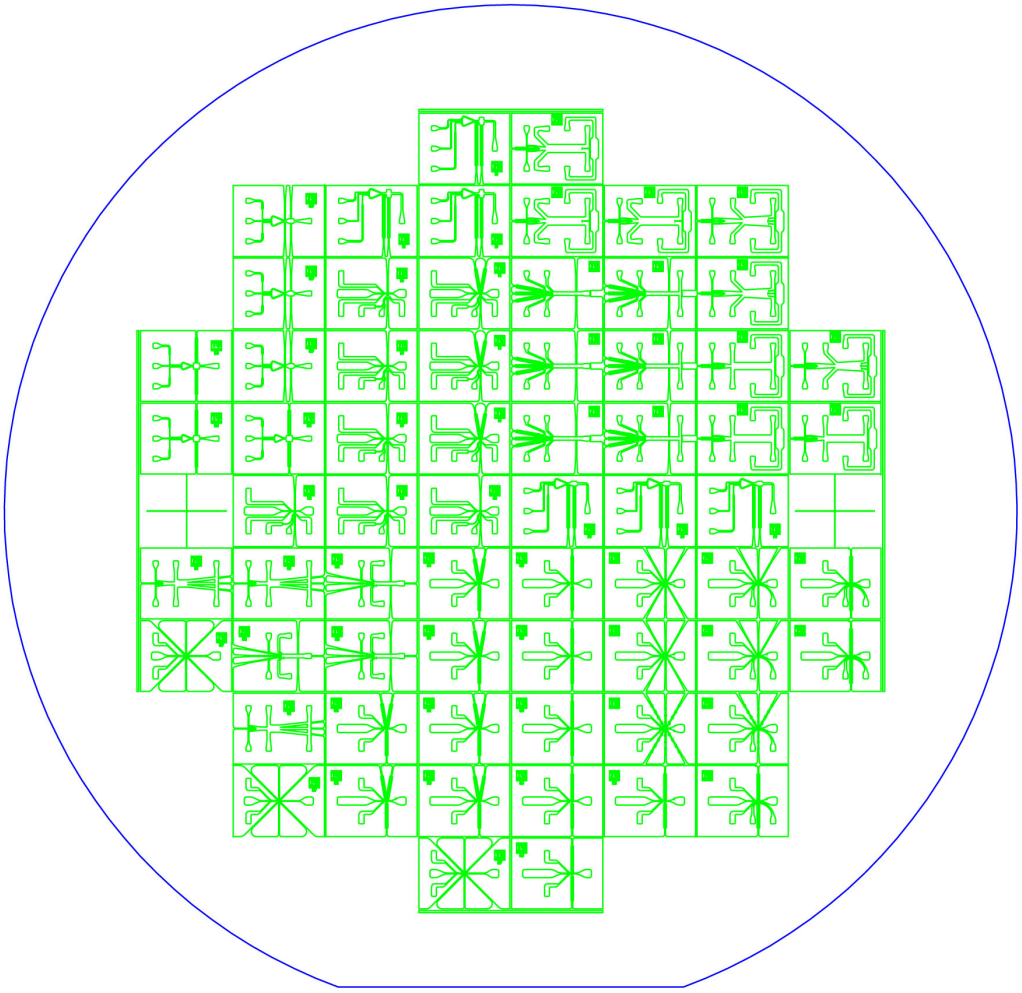

Figure A.4: Mask for structuring the SU-8 layer of wafer two

Literature

[BS06] Berthier, J. ; Silberzan, P.: *Microfluidics for Biotechnology.* Artech House, Inc., 2006

[DFL+98] Du, H. ; Fuh, R. A. ; Li, J. ; Corkan, A. ; Lindsey, J. S.: PhotochemCAD: A computer-aided design and research tool in photochemistry. *Photochemistry and Photobiology* 68 (1998), pp. 141–142

[For01] Fornel, F. d.: *Evanescent Waves - From Newtonian Optics to Atomic Optics.* Springer, 2001

[LH89] Loose, W. ; Hess, S.: Rheology of Dense Model Fluids via Nonequilibrium Molecular Hydrodynamics: Shear Thinning and Ordering Transition. *Rheologica Acta* 28 (1989), pp. 91–101

[LWL+08] Li, X. C. ; Wu, J. ; Liu, A. Q. ; Li, Z. G. ; Soew, Y. C. ; Huang, H. J. ; Xu, K. ; Lin, J. T.: A liquid waveguide based evanescent wave sensor integrated onto a microfluidic chip. *Applied Physics Letters* 93 (2008), pp. 193901/1–193901/3

[NW02] Nguyen, N. T. ; Wereley, St. T.: *Fundamentals and Applications of Microfluidics.* Artech House, Inc., 2002

[PBKP08] Pais, A. ; Banerjee, A. ; Klotzkin, D. ; Papautsky, I.: High-sensitivity, disposable lab-on-a-chip with thin-film organic electronics for fluorescence detection. *Lab on a Chip* 8 (2008), pp. 794–800

[Pär07] Pärr, Günther: *Microdevices for Realisation of Coaxial Sheath Flows*, Technical University of Vienna, Master-Thesis, 2007

[Rei05] Reider, G. A.: *Photonok - Eine Einführung in die Grundlagen.* SpringerWien-NewYork, 2005

[RV09] Rosenauer, M. ; Vellekoop, M. J.: 3D fluidic lens shaping-A multiconvex hydrodynamically adjustable optofluidic microlens. *Lab on a Chip* 9 (2009), pp. 1040–1042

[SSLV04] Svasek, P. ; Svasek, E. ; Lendl, B. ; Vellekoop, M. J.: Fabrication of miniaturized fluidic devices using SU-8 based lithography and low temperature bonding. *Sensors and Actuators A* 115 (2004), pp. 591–599

[ZT00] Zienkiewicz, O. C. ; Taylor, R. L.: *The finite element method - Fluid dynamics.* Butterworth-Heinemann, 2000